scientific reports

Check for updates

OPEN

Exploring potential diagnostic markers and therapeutic targets for type 2 diabetes mellitus with major depressive disorder through bioinformatics and in vivo experiments

Yikai Zhang[1,4], Linyue Wu[1,4], Chuanjie Zheng[1,4], Huihui Xu[2,4], Weiye Lin[3], Zheng Chen[1], Lingyong Cao[1]✉ & Yiqian Qu[1]✉

Type 2 diabetes mellitus (T2DM) and Major depressive disorder (MDD) act as risk factors for each other, and the comorbidity of both significantly increases the all-cause mortality rate. Therefore, studying the diagnosis and treatment of diabetes with depression (DD) is of great significance. In this study, we progressively identified hub genes associated with T2DM and depression through WGCNA analysis, PPI networks, and machine learning, and constructed ROC and nomogram to assess their diagnostic efficacy. Additionally, we validated these genes using qRT-PCR in the hippocampus of DD model mice. The results indicate that UBTD1, ANKRD9, CNN2, AKT1, and CAPZA2 are shared hub genes associated with diabetes and depression, with ANKRD9, CNN2 and UBTD1 demonstrating favorable diagnostic predictive efficacy. In the DD model, UBTD1 ($p > 0.05$) and ANKRD9 ($p < 0.01$) were downregulated, while CNN2 ($p < 0.001$), AKT1 ($p < 0.05$), and CAPZA2 ($p < 0.01$) were upregulated. We have discussed their mechanisms of action in the pathogenesis and therapy of DD, suggesting their therapeutic potential, and propose that these genes may serve as prospective diagnostic candidates for DD. In conclusion, this work offers new insights for future research on DD.

Keywords Diabetes with depression, Major depressive disorder (MDD), Type 2 diabetes mellitus, Machine learning, Bioinformatics analysis, Diagnosis learning, GEO database

The global health community is increasingly concerned about the rising incidence of Type 2 diabetes mellitus (T2DM) and Major Depressive Disorder (MDD). The International Diabetes Federation predicts that the number of adults with diabetes will reach 642 million by 2040[1], and the World Health Organization reports that over 264 million people were living with depression in 2019[2]. The simultaneous occurrence of these conditions is particularly concerning, as they exacerbate each other's harmful effects, resulting in increased morbidity and mortality.

The interplay between T2DM and MDD is well-documented, with each condition increasing the risk of the other[3]. However, the biological mechanisms driving this comorbidity remain a subject of ongoing research and debate. Research suggests that insulin resistance and inflammation contribute to depression in T2DM patients[4], while other studies highlight psychosocial factors and genetic predispositions[5]. This complexity is underscored by the varied clinical responses to treatment, where some patients improve with antidepressants and lifestyle changes, while others do not[6].

Despite growing awareness of the need to address the comorbidity of T2DM and MDD, consensus on the most effective treatment strategies remains unattainable. Advocates for an integrated approach support collaborative

[1]School of Basic Medical Sciences, Zhejiang Chinese Medical University, Hangzhou 310053, Zhejiang, China. [2]Institute of Orthopedics and Traumatology, Zhejiang Provincial Hospital of Chinese Medicine, The First Affiliated Hospital of Zhejiang Chinese Medical University, Hangzhou, China. [3]The First College of Clinical Medicine, Zhejiang Chinese Medical University, Hangzhou, China. [4]Yikai Zhang, Linyue Wu, Chuanjie Zheng and Huihui Xu contributed equally to this work. ✉email: caolingyong@163.com; 20221029@zcmu.edu.cn

care models involving both endocrinologists and mental health professionals[7]. Conversely, some suggest that targeting pathophysiological mechanisms like endoplasmic reticulum stress or neuroinflammation could offer more effective management strategies[8].

In this study, we explored the complex link between T2DM and MDD, identifying shared hub genes (UBTD1, ANKRD9, CNN2, AKT1, CAPZ2A) that may serve as diagnostic markers for their comorbidity. This discovery is crucial for improving clinical management, patient outcomes, and reducing the societal burden. Our findings pave the way for more precise diagnostics and personalized treatment strategies. Further research is needed to validate the diagnostic potential of these genes and assess their clinical impact.

Materials and methods

Microarray data and sample size calculation

We retrieved gene expression profiling data from the Gene Expression Omnibus (GEO) DATABASE (https://www.ncbi.nlm.nih.gov/geoprofiles/. Accessed 25 August 2024) for patients with diabetes and depression (GSE26168, GSE15932, GSE53987, GSE66937). GSE26168 includes 9 T2DM patient samples and 8 control samples. GSE15932 comprises 8 T2DM samples and 8 control samples. GSE53987 consists of 17 MDD patient samples and 18 control samples. GSE66937 contains 9 suicide completers and 7 control samples. These samples were used in subsequent analyses, and their specific accession numbers are available in Supplementary Table S1. Given the limited sample size in some arrays, we performed a combined analysis across multiple chips for the same disease condition. Due to the relatively limited sample size in individual T2DM datasets, we chose to combine multiple datasets (GSE26168 and GSE15932) and then carried out rigorous data normalization and batch effect correction procedures. In the course of this process, one sample (GSM532824 from GSE26168) was excluded to maintain the highest standards of data quality and integrity.

Additionally, For the data processing, we utilized the limma package (version 3.58.1) in R (version 4.3.2) to standardize and correct all the data. Gene names were annotated using the AnnoProbe package (version 0.7.1) to ensure accurate identification. To address the batch effects arising from different platforms more comprehensively, we employed the SVA package (version 3.50.0) to remove these discrepancies. The co-expressed genes identified were further subjected to validation using independent datasets to ascertain their expression in tissues. As these datasets are publicly available, ethical approval was not required.

Data processing and identification of differentially expressed genes (DEGs)

We extracted raw data and performed background correction, normalization, and log2 transformation using the R software package (version 4.3.2). When multiple probes corresponded to the same gene symbol, we calculated the average expression level to complete the data processing procedure. The Limma R software package was employed to identify DEGs associated with depression. For the T2DM dataset, we set a threshold of $p < 0.05$ and $|\log2 \text{ Fold Change}| > 1$ to select differentially expressed genes (DEGs). For the MDD dataset, we applied a criterion of $p < 0.05$ and $|\log2 \text{ Fold Change}| > 0$ to identify DEGs[9].

T2DM weighted gene co-expression network analysis (WGCNA)

Weighted gene co-expression network analysis (WGCNA) is a systems biology approach utilized to construct gene co-expression networks and evaluate gene network modules associated with diseases. We employed the WGCNA package in R to build a co-expression network for the top 5000 expressed genes. A weighted adjacency matrix was constructed based on the weighted correlation coefficient, and the adjacency matrix was transformed into a topological overlap matrix (TOM). Subsequently, hierarchical clustering was performed to identify modules and calculate eigengenes. Finally, we assessed the correlation between phenotypes and each module through correlation analysis and identified gene-associated modules. Prior to constructing the scale-free co-expression network, the DEG expression matrix was filtered using the goodSamplesGenes function to remove genes and samples that did not meet quality standards. Utilizing the soft-thresholding power (β) derived from co-expression similarity to determine adjacency, we transformed it into a topological overlap matrix (TOM) to obtain gene proportions and associated dissimilarities. Finally, we employed hierarchical clustering to identify modules and visualized them. Using a dissimilarity measure based on the TOM with a minimum size (gene set) of 50, we performed average linkage hierarchical clustering to cluster genes with high absolute correlations into gene modules, described as a gene dendrogram. By cutting the tree at a height that maximizes module eigengene differentiation, we merged similar modules (module size > 50). The eigengene network was graphically represented.

Functional and pathway enrichment analysis

We conducted enrichment analysis to explore the functions of DEGs and obtain a more comprehensive understanding of their biological information. The ClusterProfiler package (version 4.3.2) in the R platform was utilized for Gene Ontology (GO) enrichment analysis and Kyoto Encyclopedia of Genes and Genomes (KEGG) pathway enrichment[10–12]. The results of the enrichment analysis were categorized into three functional classes: biological process (BP), cellular component (CC), and molecular function (MF). The results were visualized using barplot maps and dotplot maps. Statistical significance was defined as $p < 0.05$.

PPI network construction and hub gene selection

We utilized the STRING database (http://string-db.org. Accessed 3 September 2024) to construct a protein-p rotein interaction (PPI) network online for the genes overlapping between the WGCNA module genes and MDD's DEGs. We set the interaction score to a confidence threshold of > 0.150 and hid disconnected nodes in the network. Subsequently, to better comprehend the interrelationships between proteins and select functionally interacting hub genes, we visualized and analyzed the PPI network using Cytoscape software (version 3.7.1,

http://www.cytoscape.org/. Accessed 3 September 2024). We employed cytoHubba to rank genes within the PPI network based on MCC, MNC, Degree, EPC, and BottleNeck algorithms, identifying the top 2 ranked genes from each algorithm as potential hub genes for DD.

Machine learning algorithms for identifying potential biomarkers

We employed both Boruta and SVM-RFE algorithms to analyze T2DM and MDD datasets[13,14], aiming to identify overlapping feature genes between T2DM and MDD as potential biomarkers and hub genes for DD. For Boruta implementation, shadow features were created by repeatedly permuting original features, with feature importance evaluated through a random forest-based approach. Following processing with the getSelectedAttributes function (withTentative = TRUE) and TentativeRoughFix function, all features labeled as "Confirmed" or "Tentative" were retained. A robust cross-validation framework was implemented using the trainControl function, employing 10-fold validation with 5 repetitions. Parameters such as boxConstraint and kernelScale were systematically adjusted to enhance model performance. To ensure the robustness of feature selection, 10-fold validation with 5 repetitions scheme was implemented using the trainControl function. Model optimization was achieved through systematic parameter tuning, including boxConstraint adjustments for margin control and kernelScale modifications for RBF kernel calibration.

The SVM-RFE algorithm employed recursive feature elimination while monitoring model performance changes, ultimately selecting the radial basis function kernel (SVM-Radial) as the classifier. Using kernel RFE with 25 features, we performed 10-fold cross-validation to systematically evaluate the impact of different feature subsets on model performance, thereby determining the optimal subset size. This configuration was implemented through the fitcsvm function with 'KernelFunction','rbf' parameters, where kernelScale and other parameters were optimized to enhance model performance.

Receiver operating characteristic curve (ROC) and nomogram construction

Evaluating the Diagnostic Efficacy of the 5 Potential Hub Genes for DD Identified from T2DM and MDD Datasets. We initially constructed receiver operating characteristic (ROC) curves and calculated the area under the ROC curve (AUC) to estimate the diagnostic value. To prevent bias, the GSE66937 dataset was employed as a validation set, and only candidates with AUC values > 0.7 in both the test and validation sets were selected. Subsequently, a nomogram was constructed using the rms R package, and the diagnostic performance of the model was verified based on AUC > 0.8.

Experimental animals

Specific-pathogen-free (SPF) male C57BL/6J mice, aged 6 weeks (20 ± 2 g), were purchased from Zhejiang Chinese Medical University (Hangzhou, China). All mice were housed in the Laboratory Animal Center of Zhejiang Chinese Medical University under conditions of 22 ± 2 °C temperature, 50 ± 5% humidity, and a 12-hour light/dark cycle. The animal study protocol was approved by the Institutional Review Board of Animal Experiments of Zhejiang Chinese Medical University for studies involving animals. The care and use of animals were strictly in accordance with the "Guide for the Care and Use of Laboratory Animals" (Approval No., IACUC-20240122-04). All procedures were conducted in full compliance with the ARRIVE guidelines 2.0. In addition, at the conclusion of the experiment, we adhered to the American Veterinary Medical Association (AVMA) Guidelines for the Euthanasia of Animals (2020) and utilized zolazepam and tiletamine (Zoletil 50, i.p. 50 mg/kg) for the anesthesia and euthanasia of mice.

Experimental design

After a one-week acclimatization period with ad libitum feeding, mice were randomly assigned to the Control group ($n = 6$) and the Model group ($n = 6$). Mice in the Control group were fed a standard diet (SD) for 8 weeks, while those in the Model group maintained a high-fat diet (HFD) for 8 weeks. Following 8 weeks of dietary induction, mice in the Model group were intraperitoneally injected with streptozotocin (STZ) solution at a dose of 50 mg/kg/day (STZ; Sigma; Cat., ABT650-1 g), prepared in 0.1 M citrate buffer (pH 4.5) at 4 °C and protected from light (Solarbio, Cat., C1013), while mice in the Control group were intraperitoneally injected with 0.05 ml of citrate buffer per 10 g of body weight/day for 5 consecutive days. One week after the final STZ injection, mice with fasting blood glucose (FBG) ≥ 11.1 mmol/l were considered to have T2DM and continued on the HFD. This time point was designated a 0 week.

To establish a T2DM with depression model, all members of the Model group were subjected to solitary housing combined with chronic unpredictable mild stress (CUMS) to induce progression to depression in T2DM mice[15]. We followed the procedure from a previous report with moderate modifications to establish the CUMS model[16]. Briefly, each mouse in the Model group was singly housed and exposed to 10 types of mild stressors (e.g., wet pad, tail nipping, cage exchange, 45° cage tilt, cage shaking, etc.), with only one stressor applied per day and no repeated stressor within a 7-day period to ensure unpredictable stress (Table 1). The entire CUMS lasted for 4 weeks (28 days) to establish the CUMS-induced diabetes with depression (DD) mouse model. C57BL/6J mice without stress were housed undisturbed in their cages. Notably, body weight and FBG were measured weekly during the CUMS period, with FBG determined by collecting blood from the tail tip using a glucometer (ACCU-CHEK Instant, Roche, Germany). The schematic of the experimental procedure is shown in Fig. 6a.

Oral glucose tolerance test (OGTT)

The glucose tolerance test was conducted using an oral glucose tolerance test (OGTT). On the last day of CUMS (day 28), after measuring fasting blood glucose (FBG), overnight-fasted mice were administered glucose (1 g/kg) by oral gavage, and blood samples were collected from the tail vein at 0, 30, 60, 90, and 120 min for blood

Date	Stressor	Durationa
Day 1	Wet pad	24 h
Day 2	Tail nipping	3 min
Day 3	Thermal stimulation (45 °C)	5 min
Day 4	Cage exchange	24 h
Day 5	45° cage tilt	5 h
Day 6	Cage shaking	10 min
Day 7	Food deprivation	12 h
Day 8	Light stroboscopic	5 h
Day 9	Wet pad	3 min
Day 10	Tail nipping	24 h
Day 11	Thermal stimulation (45 C)	5 min
Day 12	no bedding	24 h
Day 13	45° cage tilt	5 h
Day 14	Food deprivation	12 h
Day 15	Cage exchange	24 h
Day 16	Cage shaking	10 min
Day 17	Light stroboscopic	5 h
Day 18	Wet pad	24 h
Day 19	Tail nipping	24 h
Day 20	Thermal stimulation (45 C)	5 min
Day 21	Food deprivation	12 h
Day 22	45° cage tilt	5 h
Day 23	no bedding	24 h
Day 24	Overnight illumination	12 h
Day 25	Cage shaking	10 min
Day 26	Cage exchange	24 h
Day 27	Wet pad	24 h
Day 28	Food deprivation	12 h

Table 1. CUMS proceeding.

glucose measurements using a glucometer. The area under the curve (AUC) of the OGTT was calculated using GraphPad Prism 9.5 software.

Tail suspension test (TST)

The duration of immobility in the Tail Suspension Test (TST) represents behavioral despair and the absence of escape-related activities in animals[17]. Mice were suspended approximately 2.5 cm from the tip of the tail, 40 cm above the ground, for 6 min using adhesive tape[18]. Immobility was defined as the absence of movement or only minor forelimb activity. Mice were tested individually to prevent interference. The duration of immobility was manually recorded by two experienced observers who were blinded to the group assignments[19]. Finally, the immobility period was analyzed for the last 4 min of the test by both observers.

Forced swimming test (FST)

The Forced Swimming Test (FST) is utilized to measure the despair behavior of mice in an aversive environment, thereby reflecting their level of depression[20]. Mice were placed in a cylindrical transparent container (diameter, 12 cm; height, 30 cm) filled with water at 25 ± 1 °C (25 cm deep to prevent mice from touching the bottom with their tails) and video-recorded for 6 min. During the experiment, mice were tested individually to avoid interference. Mice were considered immobile when they kept their heads above water and remained still or only slightly moved their limbs to avoid submersion[15]. Two experimenters, who were blinded to the group assignments, recorded the immobility duration from 2 to 6 min by reviewing the videos. After each test, the container was cleaned and filled with fresh warm water to prevent interference.

Organ index

After the experiment, the livers and pancreases of the mice were carefully dissected on ice and weighed. The weights of the liver and pancreas for each mouse were recorded, and the Organ index was subsequently calculated using the formula. Liver index = Liver weight (g) / Body weight (g). Pancreas index = Pancreas weight (g) / Body weight (g).

qRT-PCR analysis

According to the manufacturer's instructions, RNA was extracted from the mice hippocampus using TRIzol (Cat., CW058; CWbio; China) and its quality was assessed using a Nanodrop spectrometer. Reverse transcription

to cDNA was performed using a reverse transcription kit (Cat., Q1007A; UG Bio; China). Quantitative real-time PCR (qRT-PCR) was conducted using uGreener Flex qPCR 2X MIX (Cat., Q0005A; UG Bio; China). The relative expression levels of each target gene were normalized against β-actin expression levels, and the relative expression of the target genes was calculated using the 2-ΔΔCt method. Table 2 presents the primer sequences utilized in this study, which were synthesized by Tsingke Biotech (China).

Statistical analysis

Statistical analysis and visualization were performed using GraphPad Prism 9.5 software. To compare two experimental groups, an unpaired t-test was employed, and all data are presented as mean ± standard error of mean (S.E.M.). Additionally, for the analysis of Body Weight and FBG changes at different time points, a two-way ANOVA was conducted followed by Sidak's multiple comparisons test. The significance level was set at $\alpha = 0.05$, and a p value < 0.05 was considered statistically significant.

Results

Identification of T2DM-associated gene modules

Normalization of expression values in the T2DM dataset (GSE26168 and GSE15932) was performed using Principal Component Analysis (PCA). Data before and after normalization are presented in Supplementary Fig. S1. By integrating gene expression data with clinical traits, WGCNA constructs a co-expression network to identify key modules implicated in critical biological processes. Our application of WGCNA analysis revealed interconnected gene clusters or modules with significant association to T2DM. The most acceptable soft threshold power, $\beta = 9$, was selected on the basis of scale independence and average connectivity (Fig. 1a). We delineated the cluster tree for both the T2DM cohort and the control group (Fig. 1b–d). Post-module consolidation, we identified 18 gene co-expression modules associated with T2DM, each represented by a unique color (Fig. 1e). Notably, the MEPurple ($r = 0.50$, $p = 0.004$), MEcyan ($r = 0.56$, $p = 9e^{-04}$), MERed ($r = 0.57$, $p = 6e^{-04}$), MEturquoise ($r = 0.39$, $p = 0.03$), MEGreen ($r = 0.38$, $p = 0.03$), and MElightGreen ($r = 0.38$, $p = 0.03$) modules demonstrated positive correlations with T2DM. In contrast, the MEmegenta ($r = -0.51$, $p = 0.003$), MEmidnightblue ($r = -0.75$, $p = 6e^{-07}$), and MEbrown ($r = -0.37$, $p = 0.04$) modules exhibited negative correlations with T2DM. We selected six positively correlated modules and three negatively correlated modules for further in-depth analysis, encompassing 1361 and 736 genes, respectively.

Identification of differentially expressed genes (DEGs) asociated with MDD

Utilizing the limma package, we identified 672 differentially expressed genes (DEGs) between the control and depression groups, with 375 upregulated and 297 downregulated. These DEGs were visualized as a heatmap (Fig. 2a), where red and blue represent upregulated and downregulated DEGs, respectively. Additionally, all DEGs were plotted on a volcano plot to reflect their fold change and statistical significance (Fig. 2b), with upregulated and downregulated genes marked in red and blue, respectively. Subsequently, we intersected the 375 upregulated DEGs with the 1361 genes from the T2DM positively correlated modules and the 297 downregulated DEGs with the 736 genes from the T2DM negatively correlated modules, obtaining 19 and 6 shared genes, respectively (Fig. 2c, d). These 25 genes, which are both part of T2DM-related modules and differentially expressed between MDD patients and healthy individuals, were used to characterize a gene set closely associated with the pathogenesis of DD for further analysis (These 25 genes are also referred to as DD potential genes, DDPGs).

Enrichment analysis and hub gene selection based on DDPGs

We conducted enrichment analysis on the 25 DDPGs using GO and KEGG annotations. The GO enrichment analysis revealed that the DDPGs were primarily enriched in the following categories: (1) MF: molecular function regulator activity, protein-containing complex binding, molecular function activator activity, actin filament binding, cytoskeletal protein binding, actin binding; (2) CC: myofibril, cell cortex, sarcomere, I band, Z disc, cortical cytoskeleton, cluster of actin-based cell projections, supramolecular complex, supramolecular

Gene	Primer sequence (5'→3')
UBTD1-F	GAGCTCTCGATGTCGGGCTG
UBTD1-R	CTTCTTCAAGGGCTCATTGCG
CNN2-F	GTGTGGGCTTTGGGGTTTTC
CNN2-R	GTCTGGTGGGTCAATCCTGG
AKT1-F	CATGCAGCACCGGTTCTTTG
AKT1-R	TAGGAGAACTTGATCAGGCGG
CAPZA2-F	ACTGCACTGCGAGCTTATGT
CAPZA2-R	CCACTCTGACCTCCAACGAC
ANKRD9-F	TGTTGGGTGAGGACAAGTTC
ANKRD9-R	GATGGCAGAGGCAGTTCAT
β-actin-F	CACCCGCGAGTACAACCTTC
β-actin-R	CCCATACCCACCATCACACC

Table 2. Primer sequence used for qRT-PCR.

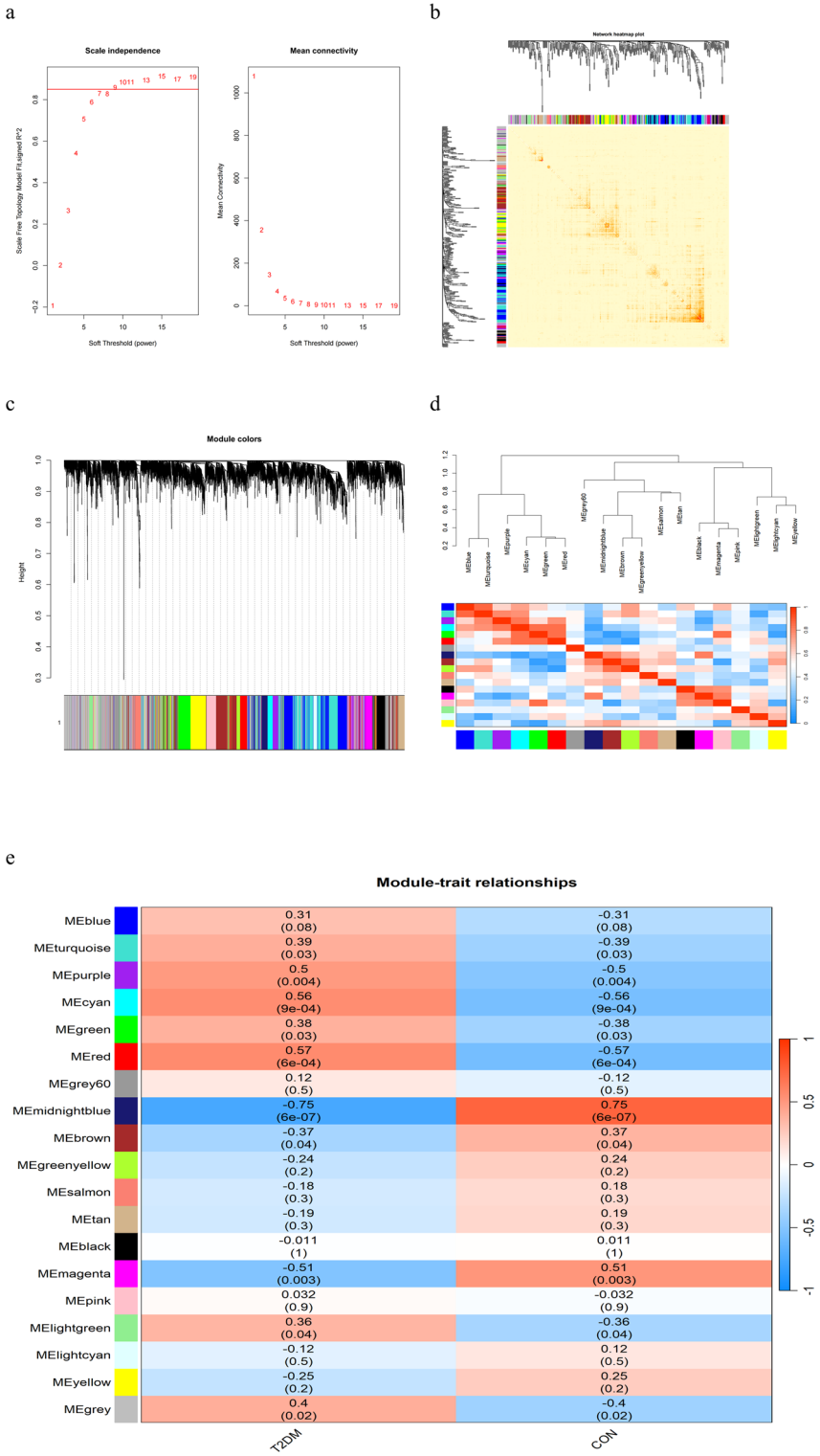

Fig. 1. Identification of T2DM-associated gene modules (a) Soft threshold capability (β) selection by scale independence and mean connectivity. (b) Network heat map showing gene tree and module characteristic genes. (c) The gene clusters or modules associated with T2DM are shown in different colors under the cluster tree. (d) Network heat map showing gene tree and module characteristic genes. E. Heat maps revealing the relationship between module feature genes and T2DM status. The correlation and *p*-values of module characteristic genes and T2DM status are described.

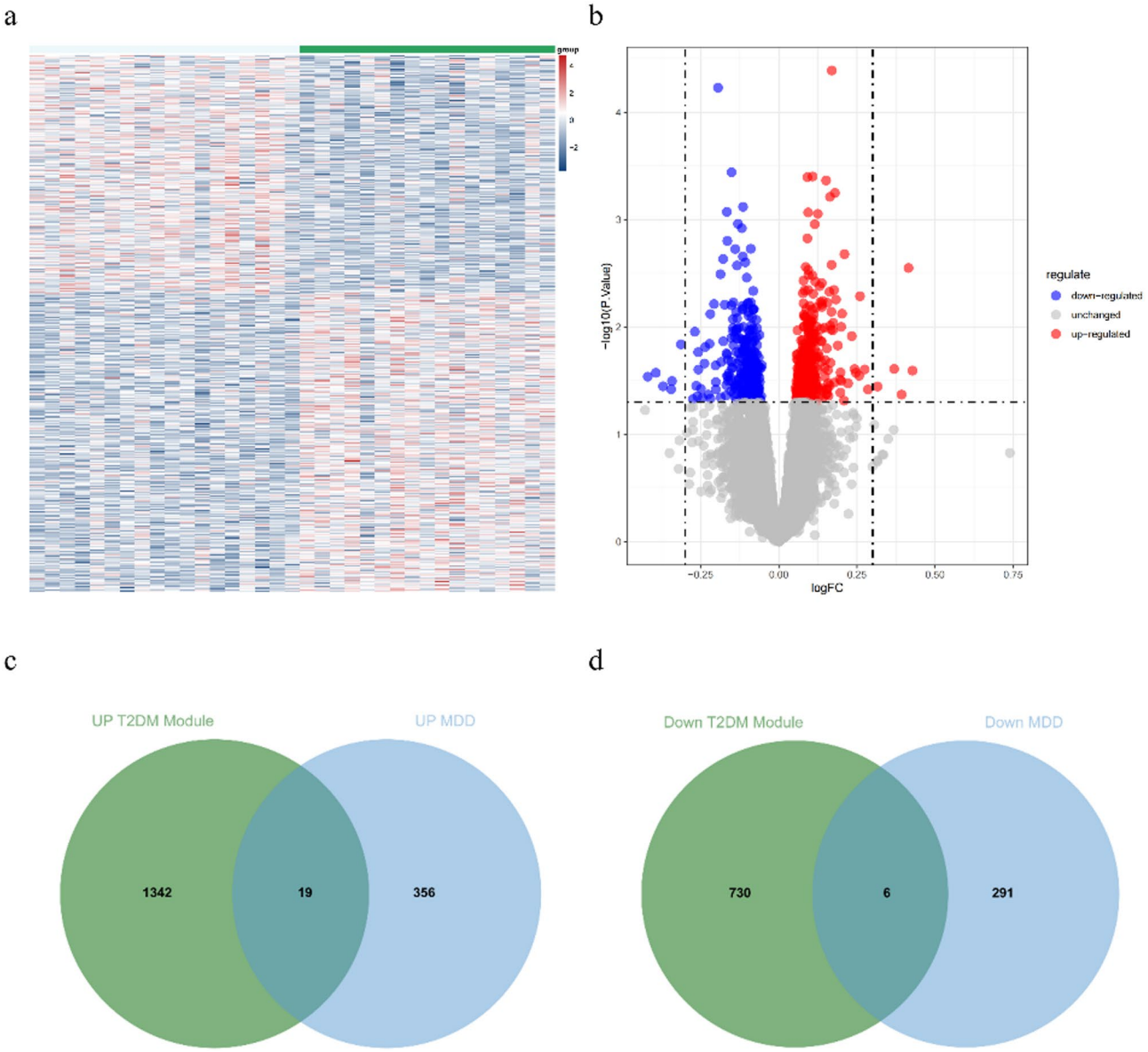

Fig. 2. Identification of DEGs associated with MDD. a. Heat maps of up-regulated and down-regulated DEGs detected between the MDD and CON groups. The red and blue grids represent up-regulated and down-regulated DEGs, respectively. b. Volcanic maps of all DEGs, red and blue indicate up-regulated and down-regulated DEGs, respectively. c-d. The intersection of WGCNA-identified T2DM associated module genes with limma detected DEGs associated with MDD progression was visualized using Venn diagrams.

fiber, supramolecular polymer; (3) BP: regulation of muscle contraction, regulation of protein depolymerization, negative regulation of protein depolymerization, negative regulation of protein-containing complex disassembly, actin filament capping, negative regulation of actin filament polymerization, negative regulation of actin filament depolymerization, regulation of actin filament depolymerization, actin filament-based process, regulation of actin filament-based process (Fig. 3a). The KEGG pathway enrichment analysis showed that these genes were mainly enriched in the Toll-like receptor signaling pathway, Lipid and atherosclerosis, Cytoskeleton in muscle cells, Chemokine signaling pathway, and C-type lectin receptor signaling pathway (Fig. 3b). These results indicate that the DDPGs play crucial roles in the maintenance of the cytoskeleton, signal transduction, immune response, lipid metabolism, and dynamic changes of macromolecular polymers. Due to the small sample size, the p-values for the enriched pathways did not reach statistical significance. This is likely because the small number of genes did not provide enough statistical power to detect significant enrichments. Therefore, the results should be interpreted with caution, and further validation with a larger gene set is recommended. Subsequently, we constructed a PPI network based on the 25 DDPGs (Fig. 3c). To assess how important these genes are in the complex network, we use cytoHubba to compute the network ranking of individual nodes. The network consists of 23 nodes and 32 edges. Nodes represent proteins encoded by genes, and lines represent interactions between proteins. We arranged these nodes in two concentric circles based on Degree, with the central node having the

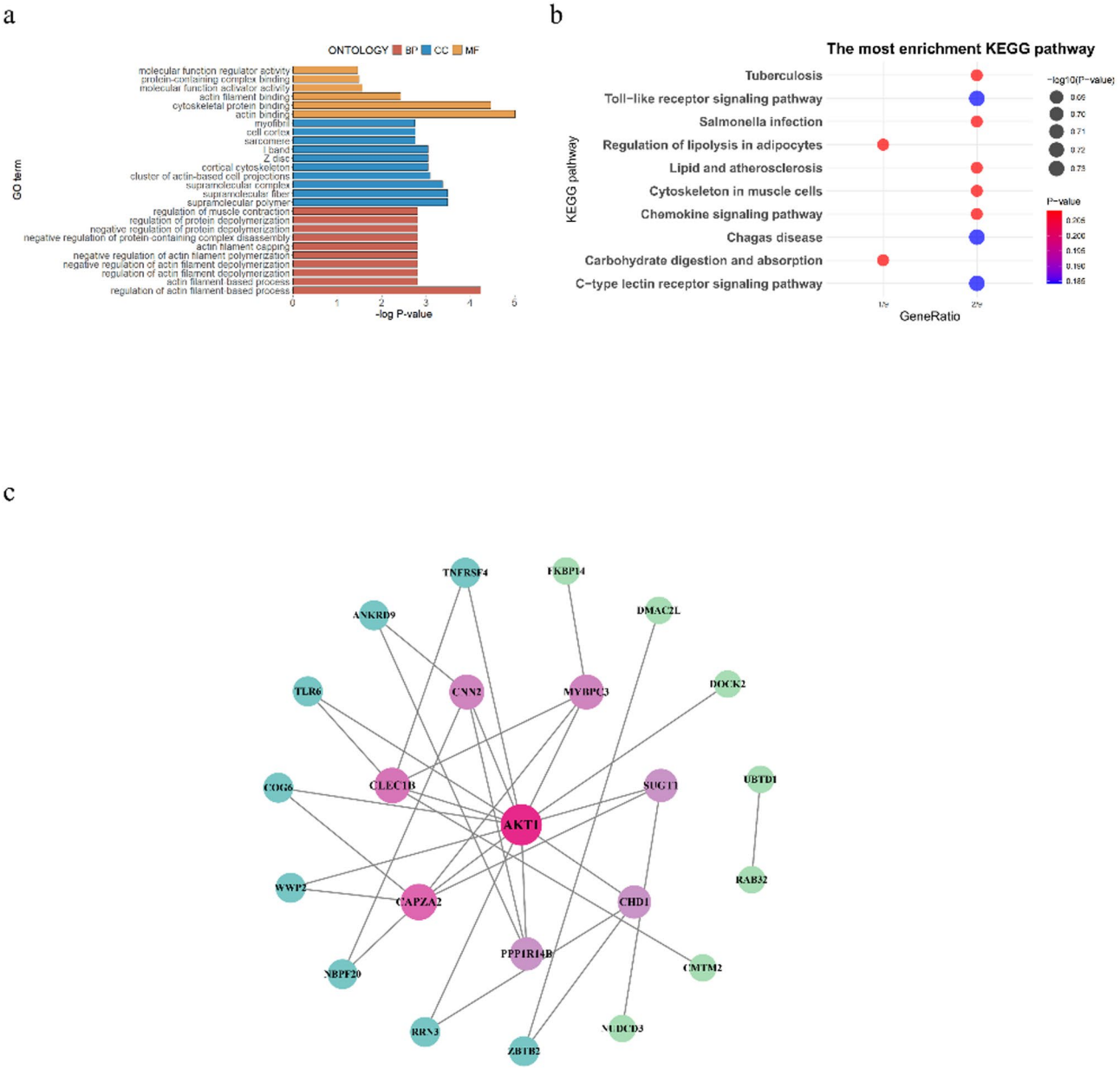

Fig. 3. Enrichment analysis and hub genes selection based on DDPGs. (a) GO analysis of DDPGs. The red, blue, and orange bar charts represent Biological Process (BP), Cellular Component (CC), and Molecular Function (MF), respectively. The length of the bar chart represents -log10 (P-value), with higher values indicating more significant enrichment. The top 6 terms for MF and the top 10 terms for BP and CC are displayed according to significance. (b) KEGG analysis of DDPGs. The x-axis of the bubble chart represents the GeneRatio of DDPGs enriched in that entry. Bubbles of different colors and sizes represent the P-value and -log10 (P-value) of the enriched entry, indicating its significance. The top 10 entries are displayed according to significance. (c) PPI network of DDPGs. The nodes represent proteins encoded by genes, and the lines represent interactions between proteins. The color of the nodes, including red and green, and their shades, indicate the size of the Degree. (DDPGs, DD potential genes)

highest Degree of 13. The red nodes in the smaller circle have a Degree of 3–6, and the green nodes in the larger circle have a Degree of 1–2. The color intensity represents the size of the Degree. We ranked the 25 DDPGs based on the Degree, MCC, MNC, EPC, and BottleNeck algorithms (Supplementary Table S2). Notably, 2 DDPGs (AKT1 and CAPZA2) consistently ranked in the top two across all five algorithms. Therefore, we designated these two DDPGs as potential biomarkers hub genes in DD.

Identification of candidate diagnostic biomarkers for DD based on machine learning

Machine learning algorithms, leveraging principles such as feature selection and pattern recognition, can process high-dimensional data to identify features associated with a given task[21,22]. In the T2DM dataset,

SVM-RFE and Boruta algorithms selected 13 and 9 characteristic genes, respectively (Fig. 4a, c). In the MDD dataset, SVM-RFE and Boruta algorithms identified 15 and 11 characteristic genes, respectively (Fig. 4b, d). Subsequently, Venn diagrams were used to identify 5 overlapping characteristic genes between T2DM and MDD (UBTD1, ANKRD9, NUDCD3, CNN2, and FKBP14, Fig. 4e). Furthermore, to emphasize the superior accuracy and good interpretability of machine learning-identified characteristic genes as disease biomarkers, we further

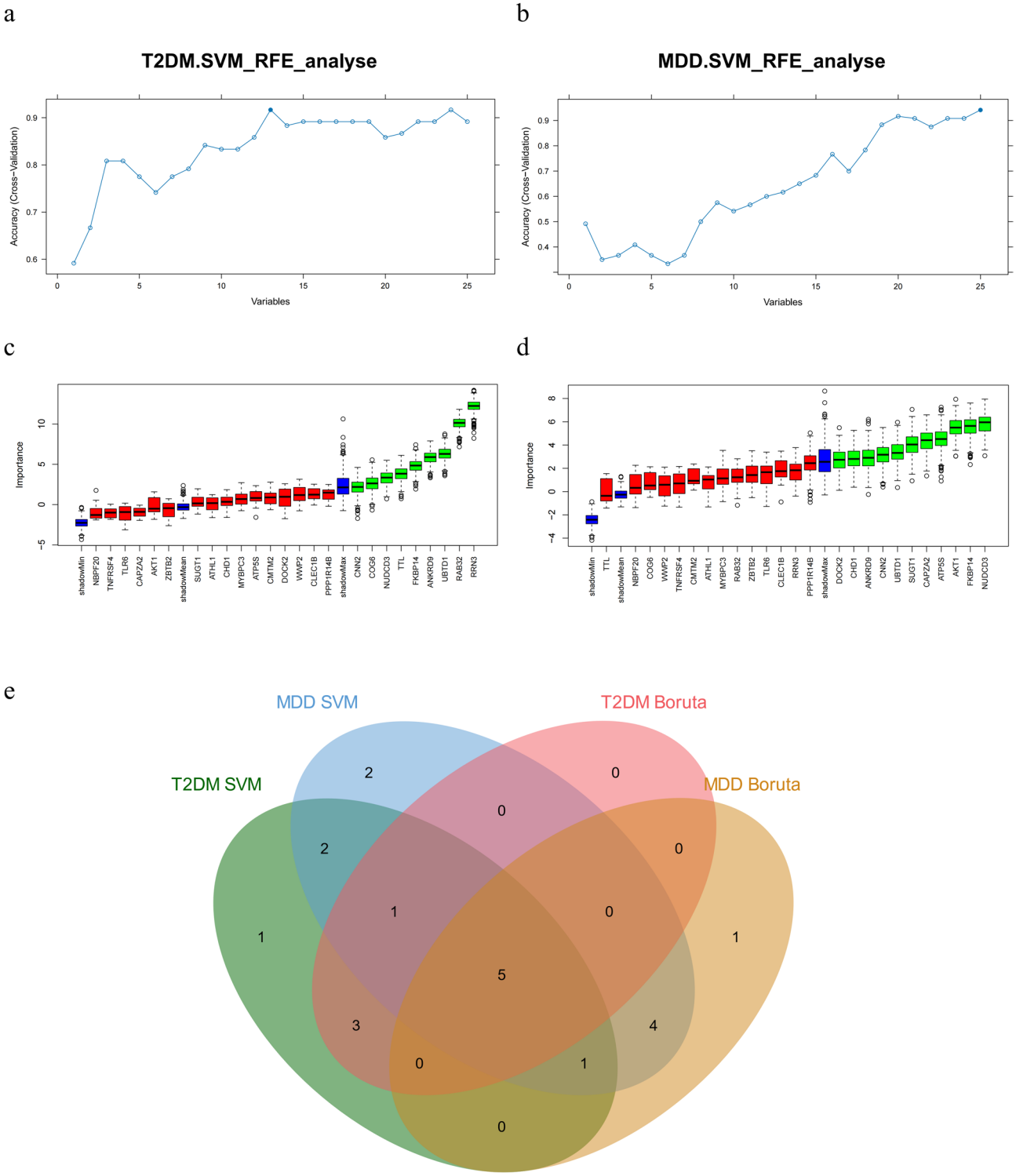

Fig. 4. Identification of candidate diagnostic biomarkers for DD based on machine learning. a, b. In the T2DM and MDD datasets, candidate genes were selected by SVM-RFE. c, d. In the T2DM and MDD datasets, candidate genes were selected by scoring the importance of features by Boruta. e. Five characteristic genes were selected by the intersection of two machine learning algorithms were visualized using the Venn diagram.

examined whether the expression trends of these 5 characteristic genes were consistent in T2DM and MDD[23–25]. Ultimately, we determined that UBTD1, ANKRD9, and CNN2 exhibited consistent expression patterns in both T2DM and MDD, suggesting their potential as DD biomarkers and hub genes.

Assessment of the diagnostic efficacy of potential hub genes in DD

Utilizing PPI networks and machine learning, we identified 5 potential hub genes for DD (UBTD1, ANKRD9, CNN2, AKT1 and CAPZA2). To enhance the diagnostic and predictive capabilities for DD, we constructed ROC curves for these genes in the T2DM and MDD training sets, as well as in the MDD validation set GSE66937, and calculated their AUC values to assess their diagnostic potential (Fig. 5a–c). To achieve optimal predictive and diagnostic efficacy, we selected ANKRD9, CNN2 and UBTD1, which had AUC > 0.7 in both the training and validation sets, as the final hub genes. Subsequently, we developed nomograms based on these three genes (Fig. 5d), with the relative expression levels of each gene corresponding to a score on the nomogram. Finally, we used the total score to predict the incidence of DD progression. The nomogram's AUC = 0.89 (Fig. 5e), indicating that ANKRD9, CNN2 and UBTD1 exhibit excellent performance in diagnosing DD.

Establishment of an in vivo experimental model for DD

We established the DD mice model using STZ in combination with CUMS induction. After STZ induction of T2DM, the body weight of DD mice was lower than that of the Control group ($p > 0.05$, Fig. 6b), and the fasting blood glucose (FBG) levels were significantly increased ($p < 0.001$, Fig. 6c). Following 4 weeks of depression induction, compared to the Control group, the body weight of DD mice decreased ($p > 0.05$, Fig. 6b), and FBG levels were significantly increased ($p < 0.001$, Fig. 6C). After the depression induction period, we performed an oral glucose tolerance test (OGTT) to assess glucose regulation in both groups. The results showed that the blood glucose (BG) levels of both groups sharply increased within 30 min after oral glucose administration, reaching peak values at 30 min, and then gradually decreased (Fig. 6d). The OGTT-AUC revealed the glucose uptake and utilization capacity of the mice, with the OGTT-AUC of DD mice being significantly higher than that of the Control group ($p < 0.001$, Fig. 6d). These results indicate that DD mice have more severe glucose metabolism disorders and impaired glucose tolerance. Additionally, we calculated the liver and pancreas indices of both groups. The results showed that, compared to the Control group, the liver index of DD mice increased while the pancreas index decreased ($p > 0.05$, Fig. 6e, f). This may suggest that our DD mice may have developed severe glucose and lipid metabolism disorders, leading to liver fat accumulation and pancreatic atrophy.

To assess the depressive-like behaviors of the two groups, we conducted behavioral tests after the 4-week depression induction period. The results showed that the immobility time of DD mice in the TST was significantly higher than that of the Control group mice ($p < 0.05$, Fig. 6g), and the same trend was observed in the FST ($p < 0.001$, Fig. 6h), indicating that DD mice exhibit severe depressive-like behaviors.

Validation of hub genes in vivo using qRT-PCR

We ultimately identified 5 potential hub genes for DD through the joint analysis of T2DM and MDD datasets. To further investigate the roles of these hub genes in DD, we examined their expression in the hippocampus of Control and DD mice using qRT-PCR. The results indicate that, compared to the Control group, the expression levels of CNN2 ($p < 0.001$, Fig. 7c), CAPZA2 ($p < 0.01$, Fig. 7d), and AKT1 ($p < 0.05$, Fig. 7e) were significantly upregulated in the hippocampus of DD mice, mirroring the expression trends observed in the hippocampus of MDD patients. However, the expression levels of UBTD1 ($p > 0.05$, Fig. 7a) and ANKRD9 ($p < 0.01$, Fig. 7b) were significantly downregulated in the hippocampus of DD model mice, which is opposite to the expression trends in MDD patients. These findings indicate that, except for UBTD1, the other 4 potential hub genes for DD exhibit significant differences in expression in the hippocampus of DD mice. Although the expression trends of UBTD1 and ANKRD9 in MDD and DD are inconsistent, we believe this can be partially explained by the disease variations between T2DM, MDD, and DD, as well as the species differences between humans and mice. Ultimately, our in vivo experimental results confirm the previous bioinformatics analysis, supporting these hub genes as potential biomarkers and therapeutic targets for DD.

Discussion

Diabetes is associated with various complications[26,27], with type 2 diabetes mellitus (T2DM) being the primary driver[28]. Patients with T2DM exhibit heightened susceptibility to depression[29], a comorbidity that not only substantially compromises quality of life but may also precipitate adverse clinical outcomes, notably increased hospitalization rates and mortality[30,31]. Emerging evidence suggests a bidirectional relationship between depression and T2DM[32–35], potentially mediated by shared pathophysiological mechanisms including hypothalamic-pituitary-adrenal (HPA) axis dysregulation[36,37], sympathetic nervous system (SNS) hyperactivity[38,39], circadian rhythm disruption concomitant with metabolic dysregulation[40,41], and chronic low-grade inflammation[39,42]. These shared biological pathways, possibly involving altered central-peripheral signaling crosstalk, may constitute a mechanistic foundation for the DD. Recent investigations have further highlighted the potential pathogenic roles of insulin resistance[43,44], Gastrointestinal microbiome[45], oxidative stress burden[46], and neurostructural/functional abnormalities (particularly in the fornix, hippocampus, and prefrontal cortex) in this complex interplay[44,47].

Advances in bioinformatics and systems biology have elucidated gene expression variations and patterns that may underlie DD pathogenesis, while facilitating the identification of targets for diagnostic or therapeutic interventions. By integrating WGCNA and PPI network analyses with machine learning and network algorithms, we identified five potential hub genes for DD and assessed their diagnostic efficacy based on T2DM and MDD datasets. Among these, four genes (UBTD1, ANKRD9, CNN2, and CAPZA2) were first reported in T2DM, MDD, and DD contexts, with UBTD1, ANKRD9, and CNN2 demonstrating superior diagnostic performance in

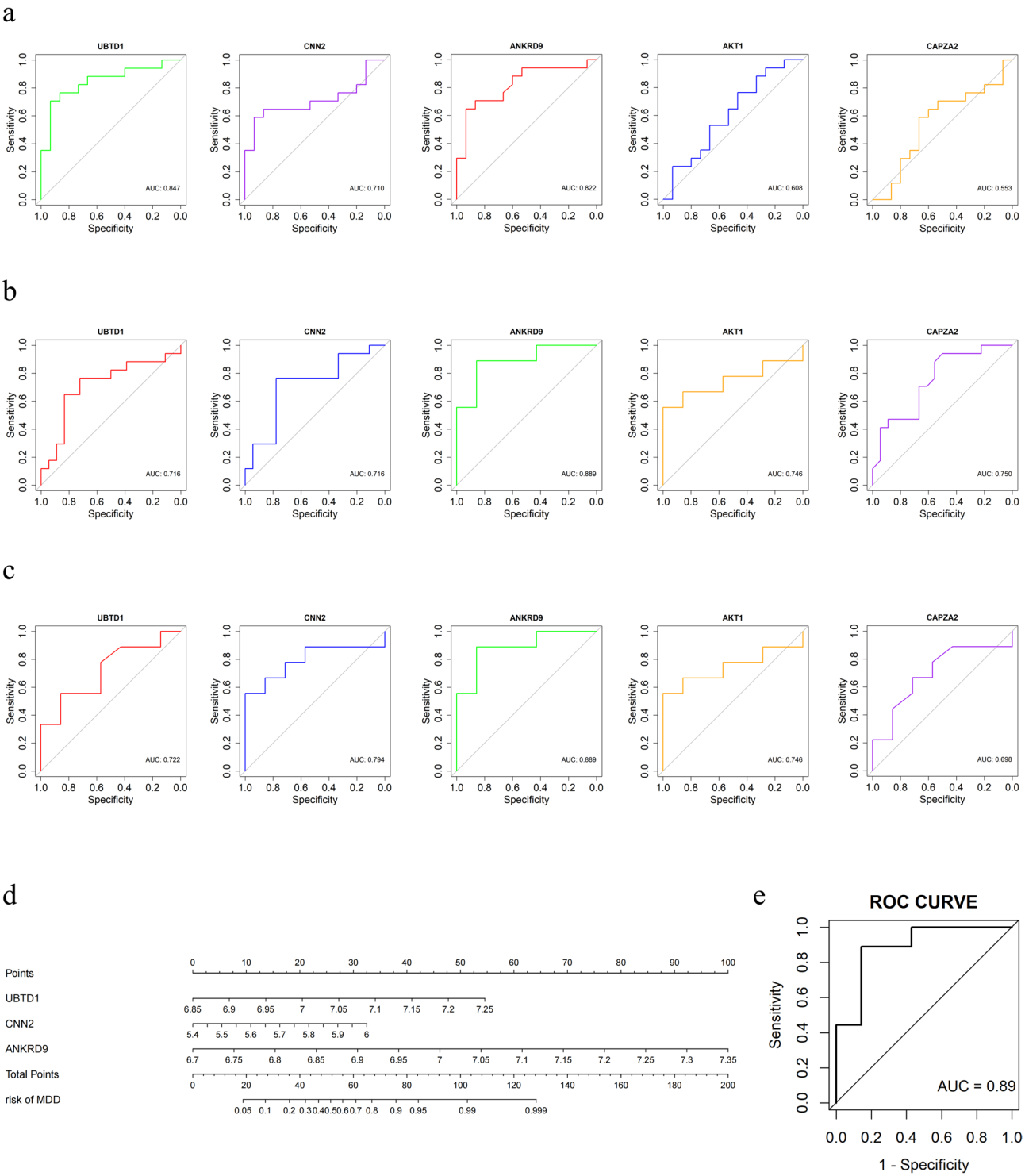

Fig. 5. Assessment of the diagnostic efficacy of potential hub genes in DD. (a) ROC curves for 5 potential hub genes of DD in the T2DM. (b) ROC curves for 5 potential hub genes of DD in the MDD. (c) ROC curves of 5 potential hub genes for DD in the MDD validation set. (d) Establish a nomogram based on 3 selected candidate biomarkers, with one score for each candidate biomarkers. (e) ROC curve of the diagnostic model for 3 selected candidate biomarkers.

simulated DD models. These findings provide mechanistic insights into DD, offering new perspectives for early identification, clinical diagnosis, and therapeutic development.

UBTD1 is a highly conserved ubiquitin-like protein that interacts with E2 and E3 enzymes in the ubiquitin-proteasome system (UPS), participating in protein degradation and functional modulation[48,49]. Current research on UBTD1 primarily focuses on oncology, with studies demonstrating its expression strongly correlates

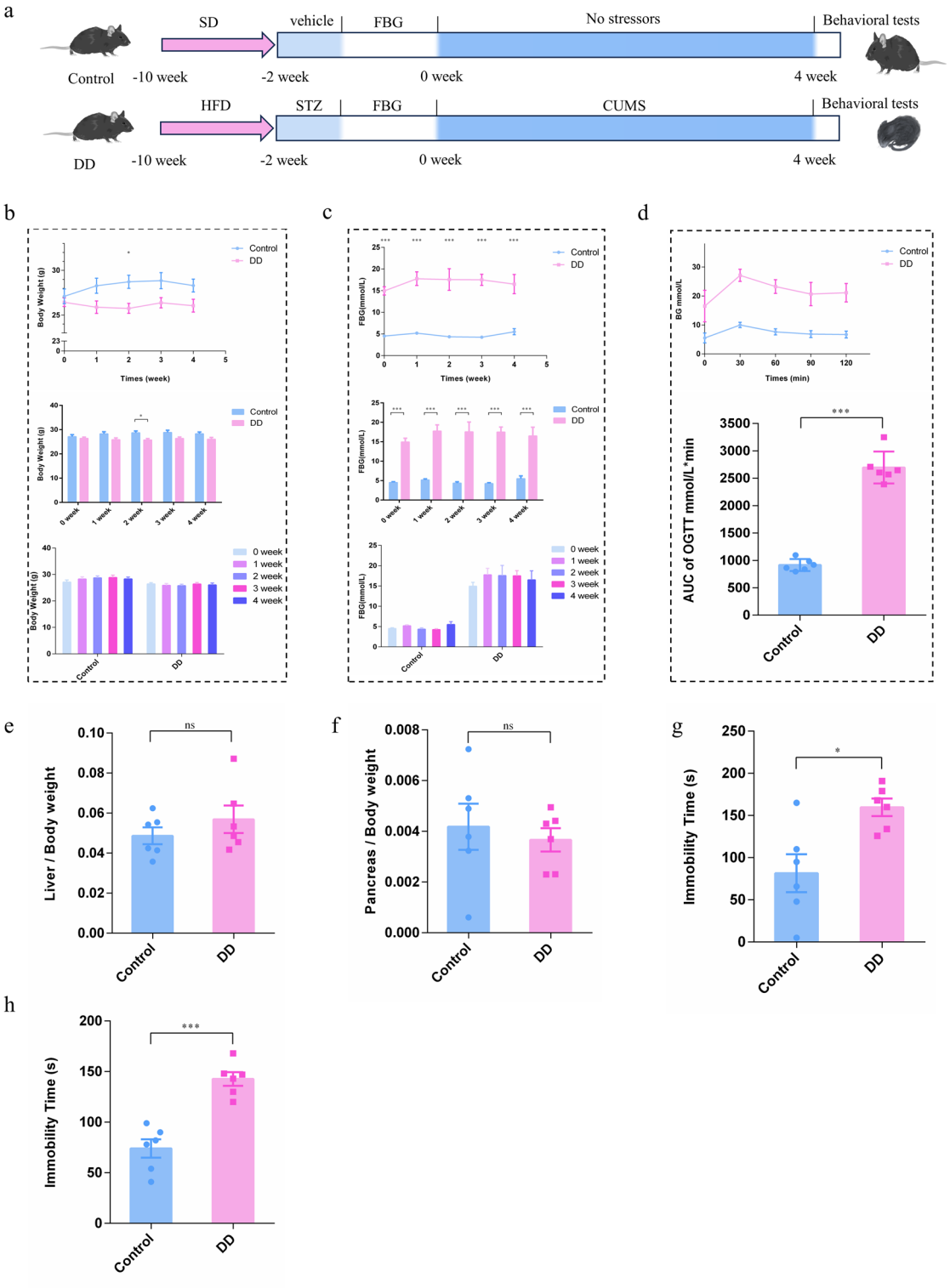

Fig. 6. Assessment of diabetic status and depressive-like behaviors in DD mice (a) Animal experimental protocol of this study. (b) Body weight of each mouse was recorded every 7 days during the experiment ($n = 6$). (c) The fasting blood glucose (FBG) of mice in different groups ($n = 6$). (d) For oral glucose tolerance test (OGTT), all mice were fasted overnight and gavaged with glucose (1 g/kg), then the tail vein blood glucose was measured at 0, 30, 60, 90 and 120 min after gavage, the bar graph represents average area under the curve ($n = 6$). e–f. Liver index and Pancreas index of DD mice ($n = 6$). g-h. The tail suspension test (TST) and forced swimming test (FST) of the immobility time of each mouse ($n = 6$). All data are presented as means ± S.E.M. Compared with the Control group, $^{*}P < 0.05$, $^{**}P < 0.01$, $^{***}P < 0.001$.

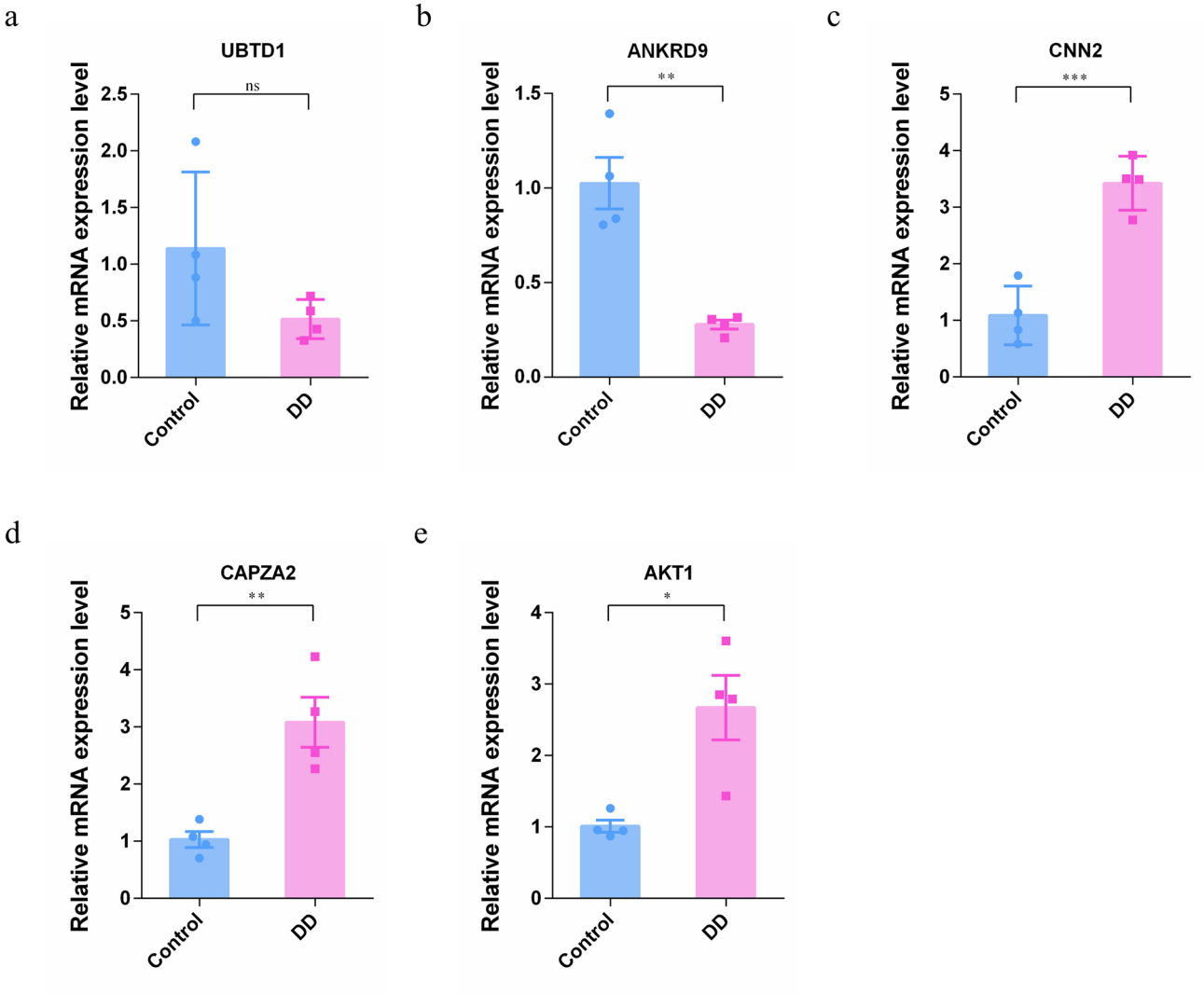

Fig. 7. Validation of hub genes in DD mice. a–e. UBTD1, ANKRD9, CNN2, CAPZA2 and AKT1 relative mRNA expression level in hippocampus of DD mice ($n = 4$). All data are presented as means ± S.E.M. Compared with the Control group, $^{*}P < 0.05$, $^{**}P < 0.01$, $^{***}P < 0.001$.

with tumor prognosis[50–53]. For instance, Zhao L et al. and Zhao Z et al. observed significantly elevated UBTD1 expression in colorectal cancer (CRC) tissues compared to adjacent normal tissues, associating high UBTD1 levels with poorer survival rates and adverse clinical features in CRC patients[50,54]. Conversely, other studies report UBTD1 downregulation in human malignancies, linking reduced expression to enhanced cancer cell invasiveness, aggressive clinical progression, and diminished overall survival[51–53]. This paradoxical expression pattern suggests UBTD1 may influence cellular fate through multiple pathways, potentially contributing to DD pathogenesis. Mechanistically, UBTD1 enhances p53 stability by promoting Mdm2 degradation. As a p53 downstream target, UBTD1 itself becomes activated by stabilized p53, establishing a positive feedback loop that induces cellular senescence and apoptosis[51]. This regulatory pathway suggests UBTD1 may mediate DD through p53-mediated control of cellular senescence and proliferation. Concurrently, UBTD1 knockdown reduces YAP ubiquitination-mediated degradation, leading to YAP activation[52,53]. Notably, elevated YAP protein levels in adipose tissue from T2DM patients and diet-induced insulin-resistant mouse models exacerbate diabetic nephropathy and cardiomyopathy[55–57]. YAP inhibition prevents glucose intolerance and adipose fibrosis, attenuates diabetic vascular calcification, and improves nephropathy and cardiac dysfunction in diabetic mice[58]. Furthermore, YAP regulates multiple processes implicated in depression pathogenesis[59–64], including autophagy modulation, extracellular matrix (ECM) remodeling, inflammatory responses, and oxidative stress regulation[65,66]. We propose that UBTD1 modulates diabetes-depression comorbidity through ubiquitination-dependent regulation of YAP signaling, integrating multiple biological pathways. Additionally, UBTD1's association with M2 macrophage polarization in the immune microenvironment and its regulation of glycolysis via the c-Myc/HK2 axis may represent critical nodes linking metabolic dysregulation to neuroinflammation[50,54]. The observed impaired cerebral glycolysis and heightened neuroinflammation in both depression and diabetes contexts further support UBTD1's potential role in DD pathogenesis through metabolic-inflammatory crosstalk[67,68].

ANKRD9 is a multifunctional protein that participates in various intracellular biological processes through its ankyrin repeat domain, including protein assembly, cytoskeletal interactions, post-translational modifications, and protein degradation[69–71]. It plays crucial roles in lipid metabolism, copper homeostasis, and cellular proliferation[72–74]. In both diabetes and depression, dysregulated lipid metabolism serves as a pivotal factor in disease progression[75–78]. ANKRD9 modulates lipid metabolism by regulating intracellular lipid accumulation[72], suggesting that its expression level alterations may influence the development of diabetes comorbid with depression. Knockdown of ANKRD9 reduces ATP7A copper efflux protein levels, leading to intracellular copper ion accumulation[73,79]. Notably, decreased ATP7A mRNA expression and elevated ceruloplasmin levels in MDD patients induce metabolic impairment in brain neurons[80]. Concurrently, abnormally elevated hippocampal copper levels in depressed mice suppress GluN2B and PSD95, resulting in synaptic dysfunction[81]. Increased copper levels demonstrate specific responsiveness to systemic lipid metabolism dysregulation[73]. Copper chelator treatment ameliorates insulin resistance and glucose intolerance under diabetic conditions[82]. These findings underscore the essential role of copper homeostasis in both neurological function and T2DM pathophysiology[83,84], positioning ANKRD9 as a potential mediator in DD pathogenesis through the copper homeostasis-lipid metabolism axis. ANKRD9 mRNA levels decrease during apoptosis[72], and its expression exhibits bidirectional regulation by apoptotic processes and lipid metabolism dysregulation. This regulatory characteristic may underlie the comorbidity between metabolic disorders and neurodegeneration. Our study revealed elevated UBTD1 and ANKRD9 mRNA levels in the hippocampus of MDD patients but downregulation in DD model mice, indicating context-dependent functional roles. These paradoxical observations mirror the conflicting reports on UBTD1 in cancer research and highlight the complex, multifaceted nature of UBTD1 and ANKRD9 in diabetes-depression comorbidity. The differential expression patterns across disease models suggest distinct pathophysiological roles in disease progression.

CNN2 (calponin 2), an actin filament-associated regulatory protein expressed in smooth muscle and non-muscle cells, inhibits myosin ATPase activity while stabilizing the actin cytoskeleton[85,86]. CNN2 modulates cellular mechanical tension and morphology through enhanced stabilization of the actin cytoskeleton[86]. Emerging evidence implicates CNN2 as a potential risk gene for Alzheimer's disease (AD), with its expression regulated by the upstream modulator ERK[87]. The activation of ERK signaling is crucial for mediating microglia-driven neuroinflammation in AD pathogenesis[88]. Macrophages lacking CNN2 exhibit accelerated migration rates, enhanced phagocytic activity, and reduced proinflammatory cytokine production, collectively attenuating inflammatory responses[89,90]. These findings suggest that targeting CNN2 may represent a novel therapeutic strategy for modulating neuroinflammation in DD. CNN2 also participates in lysosomal autophagy regulation through a dynamic process. During lysosomal damage, CNN2 initially co-migrates with the Arp2/3 complex to transiently stabilize actin filaments at compromised lysosomes. Subsequently, ubiquitinated CNN2 undergoes VCP/p97-mediated removal. This regulated dissociation releases stabilization activity, ultimately facilitating phagophore formation for efficient lysosomal autophagy[91,92]. Consequently, CNN2 overexpression may promote excessive autophagosome formation and exacerbate autophagic flux. Under T2DM conditions, hyperglycemia-induced excessive hippocampal autophagy potentially explains elevated CNN2 mRNA levels observed in both MDD patients and DD model mice[93]. Notably, CNN2 overexpression impedes cellular proliferation, likely through excessive cytoskeletal stabilization that leads to abnormal protein accumulation, disrupts dynamic remodeling processes, and ultimately compromises normal cell division and proliferative capacity[94,95]. Accumulation of aberrant cytoskeletal proteins has been recognized as a pathological hallmark across multiple neurodegenerative disorders[96–98]. Intriguingly, under conditions of hyperstabilized actin cytoskeleton, high-fat diet (HFD)-fed mice demonstrate impaired glucose tolerance, reduced insulin sensitivity, and prominent anhedonic, anxiety-like, and depressive behaviors[99]. Collectively, current evidence suggests CNN2 may regulate diabetes-depression comorbidity through three interconnected mechanisms: ERK signaling and macrophage activity mediated neuroinflammation, cytoskeletal stability-dependent control of cellular proliferation, and lysosomal autophagy pathway regulation.

CAPZA2 encodes the α2 subunit of the F-actin capping protein complex (CapZ), which regulates cytoskeletal dynamics by restricting actin filament elongation[100–102]. In high-fat diet (HFD)-induced rat models, CAPZA2 downregulation influences adipocyte hyperproliferation and differentiation through cytoskeletal remodeling, contributing to lipid metabolism dysregulation[103]. Actin, as the primary cytoskeletal component, provides structural support for synaptic development and plasticity, ensuring efficient postsynaptic signal transmission[104–106]. CapZ regulates dendritic spine actin dynamics to influence postsynaptic structural remodeling[107]. We therefore hypothesize that CAPZA2 upregulation may participate in DD pathogenesis through cytoskeletal remodeling-mediated lipid metabolism-synaptic plasticity pathways. The cytoskeleton additionally regulates endosomal trafficking via actin networks[108]. Studies reveal CapZ promotes endocytic vesicle fusion by modulating perinuclear actin filament density around early endosomes, while facilitating RAB5 effector recruitment (e.g., Rabex-5 and Rabaptin-5) to establish positive feedback loops that drive early endosome maturation[109]. Endosomal trafficking serves as a critical mechanism regulating neurotransmitter release, with its dysfunction being closely associated with neurodegenerative diseases and diabetes mellitus[110–112]. We propose that elevated CAPZA2 expression in DD pathogenesis may disrupt cytoskeletal homeostasis, causing endosomal trafficking impairments that affect neurotransmitter release/reuptake - particularly monoamine neurotransmitter reuptake blockade - ultimately impacting emotional regulation and stress responses.

AKT1, a pivotal isoform of protein kinase B (PKB/AKT), becomes activated in cells exposed to diverse stimuli[113,114]. Over recent decades, AKT1 has been extensively studied in T2DM research. Its phosphorylation activates multiple downstream pathways including mTOR, FoxO, GSK-3β, and NF-κB, thereby participating in T2DM pathogenesis through various biological responses such as cell survival, proliferation, glucolipid metabolism, and angiogenesis[115,116]. Under physiological conditions, AKT activation regulates systemic metabolic functions. However, pathological states like insulin resistance and glucolipid metabolic disorders lead

to AKT pathway suppression. Reactivation of this inhibited AKT pathway may alleviate obesity and insulin resistance, thereby improving T2DM[117–119].

Emerging evidence reveals AKT1-centered molecular networks critically regulate depression progression. In rat models of depression induced by olfactory bulbectomy, elevated oxidative stress suppresses the PIK3CA/AKT1 pathway, consequently impairing BDNF expression and synaptic plasticity[115]. Chronic unpredictable mild stress (CUMS) induction significantly downregulates p-Ser473-Akt1 levels, mediating depressive-like behaviors through increased proinflammatory cytokines and enhanced M1 microglial activation[120,121]. Clinical observations show reduced blood AKT1 and mTOR mRNA expression during depressive episodes in bipolar disorder (BD) patients[122]. The combined application of esketamine and electroconvulsive therapy (ECT) demonstrates significant antidepressant effects in rat models by activating the PI3K/Akt/GLT-1 signaling pathway[123]. Similarly, ketamine exerts rapid antidepressant effects through swift activation of the Akt-mTOR signaling pathway[124]. Furthermore, accumulating evidence suggests that AKT pathway activation reduces inflammatory responses and oxidative stress, enhances neurogenesis and synaptic plasticity, while reversing insulin resistance and cellular apoptosis—ultimately ameliorating depression-related (DD) phenotypes[125–131].

Intriguingly, our investigation revealed elevated AKT1 mRNA levels in the hippocampi of both depression-only patients and diabetic depression (DD) model mice. We postulate this phenomenon may correlate with depression progression stages induced by distinct experimental contexts, tissue-specific responses, or signal pathway hyperactivation.This hypothesis finds support in multiple studies. For instance, Wenqi Qiu et al. demonstrated that Xiaoyaosan (XYS) ameliorates chronic unpredictable mild stress (CUMS)-induced depressive-like behaviors and glucose tolerance susceptibility in rats through downregulation of the LepR-STAT3/PI3K pathway in the arcuate nucleus (ARC)[132]. In lipopolysaccharide (LPS)-induced depression models, hyperactivation of PI3K/Akt and its downstream mTOR signaling not only triggers excessive apoptosis but also suppresses autophagic flux, consequently enhancing M1 microglial polarization and neuroinflammation[133,134]. Li X et al. observed upregulated p-AKT expression in chronic restraint stress (CRS) models, proposing this response may serve dual purposes: mitigating secondary stress challenges and reflecting stressor-type specificity[135,136]. Concurrently, Zeng J et al. reported dramatically increased p-PI3K values in hippocampal tissues of model group mice, directly indicating PI3K/Akt pathway hyperactivation during depressive states[18]. Furthermore, we propose a compensatory hypothesis to explain elevated AKT1 mRNA levels. Under persistent stress conditions in diabetic depression (DD) pathology, hippocampal AKT1 activity becomes suppressed, resulting in diminished phosphorylation levels. These biochemical alterations may exacerbate depression progression by disrupting cellular survival mechanisms, apoptosis-autophagy balance, inflammatory responses, and synaptic formation/maintenance pathways. The organism appears to compensate through transcriptional upregulation of AKT1 to enhance protein translation and phosphorylation, thereby attempting to counteract this depression-associated "stress" state. However, sustained inflammatory microenvironments and oxidative stress may induce aberrant post-translational modifications that impair AKT1 protein activation, thereby causing "decoupling" of AKT1 signaling. This regulatory mismatch results in elevated AKT1 mRNA levels without proportional increases in functional protein activity. Within depression/DD contexts, the multilayered regulatory network encompassing gene expression control, post-translational modifications, protein stability, and protein-protein interactions becomes disrupted by pathological alterations. Consequently, despite increased AKT1 mRNA levels, its functional cellular activity remains suppressed.

In summary, we propose that the pathogenesis of DD involves intricate interactions within polygenic regulatory networks. A critical subnetwork comprising UBTD1, ANKRD9, CNN2, CAPZA2, and AKT1 exhibits core dysregulation characterized by dynamic imbalances among energy metabolism, signal transduction, and cytoskeletal organization. UBTD1 contributes to DD pathogenesis primarily through its dual regulation of YAP and p53 signaling pathways, coupled with its modulatory effects on M2 macrophage polarization. ANKRD9 directly participates in depression-like behaviors by disrupting copper homeostasis via ATP7A regulation, leading to synaptic plasticity impairment. Furthermore, copper accumulation-dependent oxidative stress inhibits AKT phosphorylation through ANKRD9, establishing a vicious cycle that exacerbates insulin resistance through combined metabolic derangements and oxidative damage. Additionally, UBTD1 may compensate for energy metabolism defects caused by AKT pathway suppression through c-Myc-mediated enhancement of glycolysis. Conversely, ANKRD9-induced lipid metabolism abnormalities likely amplify insulin resistance effects downstream of AKT signaling.

At the cytoskeletal regulation level, CNN2 potentially suppresses macrophage migration and attenuates inflammatory responses by stabilizing actin filaments. Its autophagy-related functions may synergize with CAPZA2-mediated endosomal trafficking to coordinate neurotransmitter release and uptake. CAPZA2 overexpression may excessively constrain actin filament elongation, thereby disrupting cytoskeletal dynamics and impairing AKT signaling-associated synaptic plasticity regulation. Conversely, high-fat diet (HFD)-induced CAPZA2 downregulation exacerbates metabolic disorders through aberrant adipocyte differentiation. As the central regulatory hub, diminished AKT1 phosphorylation attenuates signaling through dual cytoskeletal modulation pathways: First, weakened inhibition of GSK-3β promotes tau hyperphosphorylation and cytoskeletal disintegration[137,138], potentially driving compensatory CNN2 upregulation to enhance actin cytoskeletal stability. Second, mTOR signaling dysregulation creates autophagic-anabolic imbalance[139,140], forming a vicious cycle with CNN2-mediated lysosomal autophagy abnormalities. Therefore, we propose that the pathogenesis of DD fundamentally reflects a multidimensional regulatory network imbalance arising from the interplay between compensatory mechanisms and pathological damage. In the early stages, inhibition of the AKT pathway weakens its regulatory effects on downstream molecules such as GSK-3β, FoxO, and mTOR, triggering dual metabolic-synaptic impairments; whereas the compensatorily elevated AKT1 mRNA fails to effectively restore signaling activity under pathological microenvironmental constraints. This paradoxical coexistence of elevated AKT1 mRNA levels and functional inhibition epitomizes the organism's precarious equilibrium

between metabolic stress and neural injury. This multilevel interaction ultimately culminates in hippocampal comorbidity phenotypes characterized by energy metabolism dysregulation, copper homeostasis imbalance, neurotransmitter reuptake dysfunction, synaptic plasticity loss, and persistent inflammatory activation, thereby providing novel therapeutic entry points for precise modulation of compensatory mechanisms.

Furthermore, it is imperative to thoroughly explore the translational potential and challenges of our research, which could provide guidance for future investigations. In our current study, we observed expression changes of these genes in the hippocampus of DD mouse models. However, substantial differences exist between animal models and humans in physiology, pathology, and gene expression patterns, which may result in incomplete recapitulation of human disease complexity and inconsistencies between gene expression patterns/functional roles observed in animal models versus humans. Therefore, clinical application of these genes for diagnostic or therapeutic purposes necessitates rigorous validation through clinical trials. This process demands not only sufficient sample sizes to ensure reliability but also careful consideration of ethical implications, costs, and time constraints. For instance, developing diagnostic kits based on these genes requires multicenter clinical trials to validate their sensitivity, specificity, and clinical utility. This endeavor also requires collaboration among multidisciplinary teams, comprising clinicians, basic researchers, bioinformaticians, and pharmacologists. Moreover, when translating targeted therapeutic strategies for hub genes from animal models to clinical applications, careful evaluation of drug toxicity and side effects is essential. Given the substantial heterogeneity in genetic background and physiological status among humans, certain compounds demonstrating safety and efficacy in animal models may induce severe adverse reactions in humans, necessitating rigorous risk assessment and monitoring during clinical trials. Consequently, drug development targeting these genes must undergo stringent preclinical and clinical trial phases to evaluate both safety and efficacy. These constitute significant challenges in advancing translation from animal models to humans, demanding continuous efforts to overcome them in future research. Nevertheless, the strong diagnostic predictive performance of ANKRD9, CNN2, and UBTD1, coupled with their discussed involvement in DD pathogenesis, underscores their translational potential.

While our study has achieved significant advancements in identifying biomarkers for DD and exploring its potential pathogenic mechanisms, several limitations warrant acknowledgement.

In this study, we solely employed qRT-PCR methodology to validate hub genes. While this widely accepted quantitative analytical approach demonstrates technical reliability[141], it does not directly elucidate the biological functional implications of gene expression alterations. Current experimental evidence remains insufficient to establish direct causal links between these transcriptional changes and DD-related behavioral manifestations or metabolic phenotypes, particularly through mechanistic investigations like gene knockdown/overexpression studies. Therefore, we propose that subsequent investigations should initially implement functional experiments (e.g., gene knockout/knockdown) integrated with multi-omics datasets to comprehensively delineate the roles of hub genes in DD animal models. Building upon robust preclinical findings and established clinical research infrastructure, rigorous clinical validation should then be conducted to substantiate these discoveries. This validation framework may include, for instance, examining the expression patterns and functional contributions of these genes in human specimens. Such investigations could be operationalized through synergistic analysis of gene expression profiles in DD patients' peripheral blood, cerebrospinal fluid, or tissue samples coupled with multi-omics approaches (e.g., proteomics, metabolomics), thereby providing a systems-level perspective on their pathophysiological roles in DD.

Furthermore, limitations of Machine Learning: The predictive efficacy of machine learning models is fundamentally contingent upon both the quality and quantity of training data. In the present investigation, the utilization of a modest sample cohort may constrain model generalization capability, particularly in extrapolating findings to broader populations. Although we implemented rigorous batch effect correction and sample normalization protocols to minimize platform-specific biases, these approaches may not fully resolve inter-dataset heterogeneity[142]. Furthermore, the employment of complex architectures or high-dimensional data processing inherently carries overfitting risks that require careful mitigation. While we employed multiple safeguards—including cross-validation, feature selection algorithms, and independent validation cohorts—to alleviate this concern, residual risk of overfitting persists. This phenomenon may result in discordant performance metrics between training and novel datasets, ultimately compromising model generalizability and applicability.

In addition to the aforementioned limitations, in this study, we utilized datasets including GSE26168 and GSE15932. While these datasets demonstrate representativeness and utility within currently available resources, their limited sample sizes may affect the robustness of our findings. Therefore, we validated our findings in an independent dataset (GSE66937) and murine models, which should enhance confidence in result robustness. Future studies should employ multi-center collaborations to acquire larger human cohorts, thereby improving result reliability and generalizability.

Moreover, in our search for independent datasets to validate MDD-related gene expression patterns, we have encountered certain challenges. Currently, there are limited publicly available transcriptomic datasets specifically focusing on MDD, particularly those containing brain tissue samples. The GSE66937 dataset provides relatively abundant high-quality brain tissue samples (e.g., hippocampus), which are crucial for investigating the neuropathological mechanisms of MDD. Under these circumstances, we selected the GSE66937 dataset, which primarily focuses on suicide cases. Epidemiological studies have demonstrated that major depressive disorder (MDD) constitutes one of the most significant risk factors for suicidal behavior[143,144]. There exists a complex association between MDD and suicide, with overlapping biological mechanisms such as serotonin system dysfunction[145,146]. The utilization of suicide-related datasets may partially reflect certain pathological mechanisms underlying MDD[147,148]. We wish to emphasize that we fully recognize the incomplete equivalence between suicide cases and MDD, as they possess distinct core pathophysiological characteristics and clinical manifestations. However, given our current research samples and objectives, the selection of suicide cases as a validation dataset was partially driven by practical feasibility considerations. We acknowledge the potential

limitations of this approach. As the GSE66937 dataset primarily focuses on suicide cases, caution must be exercised when extrapolating these findings to the broader MDD patient population.

In conclusion, despite the aforementioned limitations, our study has provided valuable insights into the biomarkers and potential pathogenic mechanisms of DD. The identification of hub genes and their associated pathways has laid a foundation for future research. Further studies with larger sample sizes and more comprehensive experimental designs are warranted to validate our findings and explore the underlying mechanisms in greater depth. This will ultimately contribute to the development of more effective diagnostic and therapeutic strategies for DD.

Conclusions

Our study utilized a series of bioinformatics tools to identify five hub genes (UBTD1, ANKRD9, CNN2, AKT1, and CAPZ2A) from T2DM and MDD datasets, assessing their diagnostic efficacy in patients with these conditions. Our analysis indicates that these genes have the potential to serve as prospective diagnostic candidates for both MDD and T2DM. Furthermore, we validated the expression levels of these genes in the hippocampus of a DD mouse model, where all except UBTD1 showed significant differential expression between the DD model and normal mice. Concurrently, we explored the biological functions of these genes in DD, suggesting that their characteristics may reveal key mechanisms such as ubiquitination, cytoskeletal functions, and the AKT signaling pathway in the development of DD. In summary, our research not only provides new insights into the complex pathology of DD but also lays the groundwork for the discovery of biomarkers for DD. We believe that these genes will be a valuable resource for future studies and may guide the development of new therapeutic strategies and diagnostic tools.

Data availability

All datasets are publicly available derived from Gene Expression Omnibus databases (GEO) (https://www.ncbi.nlm.nih.gov/geo/query/acc.cgi?acc=GSE26168, https://www.ncbi.nlm.nih.gov/geo/query/acc.cgi?acc=GSE15932, https://www.ncbi.nlm.nih.gov/geo/query/acc.cgi?acc=GSE53987, and https://www.ncbi.nlm.nih.gov/geo/query/acc.cgi?acc=GSE66937). The datasets generated during and/or analysed during the current study are available from the corresponding author on reasonable request.

Received: 5 December 2024; Accepted: 5 May 2025
Published online: 15 May 2025

References

1. Ogurtsova, K. et al. IDF diabetes atlas: global estimates for the prevalence of diabetes for 2015 and 2040. *Diabetes Res. Clin. Pract.* **128**, 40–50 (2017).
2. Depressive disorder (depression). https://www.who.int/news-room/fact-sheets/detail/depression. Accessed 28 Sep 2024.
3. Alzoubi, A. et al. The bidirectional relationship between diabetes and depression: A literature review. *Korean J. Fam Med.* **39**, 137–146 (2018).
4. Duarte-Silva, E. et al. Shared metabolic and neuroimmune mechanisms underlying type 2 diabetes mellitus and major depressive disorder. *Prog Neuropsychopharmacol. Biol. Psychiatry.* **111**, 110351 (2021).
5. Eren, I., Erdi, O. & Sahin, M. The effect of depression on quality of life of patients with type II diabetes mellitus. *Depress. Anxiety.* **25**, 98–106 (2008).
6. Lin, E. H. B. et al. Relationship of depression and diabetes self-care, medication adherence, and preventive care. *Diabetes Care*. **27**, 2154–2160 (2004).
7. Saint-Pierre, C., Prieto, F., Herskovic, V. & Sepulveda, M. Team collaboration networks and multidisciplinarity in diabetes care: implications for patient outcomes. *IEEE J. Biomed. Health Inf.* **24**, 319–329 (2020).
8. Fourrier, C., Singhal, G. & Baune, B. T. Neuroinflammation and cognition across psychiatric conditions. *CNS Spectr.* **24**, 4–15 (2019).
9. Liu, X-L. & Chang, L-S. Deciphering the genetic links between psychological stress, autophagy, and dermatological health: insights from bioinformatics, Single-Cell analysis, and machine learning in psoriasis and anxiety disorders. *Int. J. Mol. Sci.* **25**, 5387 (2024).
10. Kanehisa, M. & Goto, S. KEGG: Kyoto encyclopedia of genes and genomes. *Nucleic Acids Res.* **28**, 27–30 (2000).
11. Kanehisa, M. Toward Understanding the origin and evolution of cellular organisms. *Protein Sci. Publ Protein Soc.* **28**, 1947–1951 (2019).
12. Kanehisa, M., Furumichi, M., Sato, Y., Matsuura, Y. & Ishiguro-Watanabe, M. KEGG: biological systems database as a model of the real world. *Nucleic Acids Res.* **53**, D672–D677 (2025).
13. Noble, W. S. What is a support vector machine? *Nat. Biotechnol.* **24**, 1565–1567 (2006).
14. Kursa, M. B. & Rudnicki, W. R. Feature selection with the Boruta package. *J. Stat. Softw.* **36**, 1–13 (2010).
15. Li, J. et al. The total alkaloids of Sophora alopecuroides L. improve depression-like behavior in mice via BDNF-mediated AKT/mTOR signaling pathway. *J. Ethnopharmacol.* **316**, 116723 (2023).
16. Pei, H., Shen, H., Bi, J., He, Z. & Zhai, L. Gastrodin improves nerve cell injury and behaviors of depressed mice through Caspase-3-mediated apoptosis. *CNS Neurosci. Ther.* **30**, e14444 (2024).
17. Can, A. et al. The tail suspension test. *J. Vis. Exp. JoVE* **2012**, e3769 (2012).
18. Zeng, J. et al. Xiaoyaosan Ethyl acetate fraction alleviates depression-like behaviors in CUMS mice by promoting hippocampal neurogenesis via modulating the IGF-1Rβ/PI3K/Akt signaling pathway. *J. Ethnopharmacol.* **288**, 115005 (2022).
19. Wang, H-Q. et al. Uncovering the active components, prospective targets, and molecular mechanism of Baihe Zhimu Decoction for treating depression using network pharmacology-based analysis. *J. Ethnopharmacol.* **281**, 114586 (2021).
20. Socała, K., Nieoczym, D., Wyska, E. & Wlaź, P. Effect of sildenafil on the activity of some antidepressant drugs and electroconvulsive shock treatment in the forced swim test in mice. *Naunyn Schmiedebergs Arch. Pharmacol.* **390**, 339–349 (2017).
21. Ding, X., Qin, J., Huang, F., Feng, F. & Luo, L. The combination of machine learning and untargeted metabolomics identifies the lipid metabolism -related gene CH25H as a potential biomarker in asthma. *Inflamm. Res. Off J. Eur. Histamine Res. Soc. Al.* **72**, 1099–1119 (2023).
22. Statnikov, A., Wang, L. & Aliferis, C. F. A comprehensive comparison of random forests and support vector machines for microarray-based cancer classification. *BMC Bioinform.* **9**, 319 (2008).

23. Xiong, T. et al. Single-Cell sequencing analysis and multiple machine learning methods identified G0S2 and HPSE as novel biomarkers for abdominal aortic aneurysm. *Front. Immunol.* **13**, 907309 (2022).
24. Zheng, P-F. et al. Identification of immune-related key genes in the peripheral blood of ischaemic stroke patients using a weighted gene coexpression network analysis and machine learning. *J. Transl Med.* **20**, 361 (2022).
25. Sarafidis, M., Lambrou, G. I., Zoumpourlis, V. & Koutsouris, D. An integrated bioinformatics analysis towards the identification of diagnostic, prognostic, and predictive key biomarkers for urinary bladder Cancer. *Cancers* **14**, 3358 (2022).
26. Cole, J. B. & Florez, J. C. Genetics of diabetes mellitus and diabetes complications. *Nat. Rev. Nephrol.* **16**, 377–390 (2020).
27. Moulton, C. D., Pickup, J. C. & Ismail, K. The link between depression and diabetes: the search for shared mechanisms. *Lancet Diabetes Endocrinol.* **3**, 461–471 (2015).
28. GBD 2021 Diabetes Collaborators. Global, regional, and National burden of diabetes from 1990 to 2021, with projections of prevalence to 2050: a systematic analysis for the global burden of disease study 2021. *Lancet Lond. Engl.* **402**, 203–234 (2023).
29. Nouwen, A. et al. Type 2 diabetes mellitus as a risk factor for the onset of depression: a systematic review and meta-analysis. *Diabetologia* **53**, 2480–2486 (2010).
30. Pouwer, F. Depression: a common and burdensome complication of diabetes that warrants the continued attention of clinicians, researchers and healthcare policy makers. *Diabetologia* **60**, 30–34 (2017).
31. Rosenthal, M. J., Fajardo, M., Gilmore, S., Morley, J. E. & Naliboff, B. D. Hospitalization and mortality of diabetes in older adults. A 3-year prospective study. *Diabetes Care.* **21**, 231–235 (1998).
32. Mezuk, B., Eaton, W. W., Albrecht, S. & Golden, S. H. Depression and type 2 diabetes over the lifespan: a meta-analysis. *Diabetes Care.* **31**, 2383–2390 (2008).
33. Maina, J. G. et al. Bidirectional Mendelian randomization and multiphenotype GWAS show causality and shared pathophysiology between depression and type 2 diabetes. *Diabetes Care.* **46**, 1707–1714 (2023).
34. Golden, S. H. et al. Examining a bidirectional association between depressive symptoms and diabetes. *JAMA* **299**, 2751–2759 (2008).
35. Bartoli, F. et al. Association between depression and neuropathy in people with type 2 diabetes: a meta-analysis. *Int. J. Geriatr. Psychiatry.* **31**, 829–836 (2016).
36. Champaneri, S. et al. Diurnal salivary cortisol and urinary catecholamines are associated with diabetes mellitus: the Multi-Ethnic study of atherosclerosis. *Metabolism* **61**, 986–995 (2012).
37. Stetler, C. & Miller, G. E. Blunted cortisol response to awakening in mild to moderate depression: regulatory influences of sleep patterns and social contacts. *J. Abnorm. Psychol.* **114**, 697–705 (2005).
38. Stetler, C. & Miller, G. E. Depression and hypothalamic-pituitary-adrenal activation: a quantitative summary of four decades of research. *Psychosom. Med.* **73**, 114–126 (2011).
39. Champaneri, S., Wand, G. S., Malhotra, S. S., Casagrande, S. S. & Golden, S. H. Biological basis of depression in adults with diabetes. *Curr. Diab .Rep.* **10**, 396–405 (2010).
40. Courtet, P. & Olié, E. Circadian dimension and severity of depression. *Eur. Neuropsychopharmacol. J. Eur. Coll. Neuropsychopharmacol.* **22** (Suppl 3), S476–481 (2012).
41. Gangwisch, J. E. Epidemiological evidence for the links between sleep, circadian rhythms and metabolism. *Obes. Rev. Off J. Int. Assoc. Study Obes.* **10** (Suppl 2 0 2), 37–45 (2009).
42. Li, Y. et al. Inflammation-activated C/EBPβ mediates high-fat diet-induced depression-like behaviors in mice. *Front. Mol. Neurosci.* **15**, 1068164 (2022).
43. Kan, C. et al. A systematic review and meta-analysis of the association between depression and insulin resistance. *Diabetes Care.* **36**, 480–489 (2013).
44. Ho, N., Sommers, M. S. & Lucki, I. Effects of diabetes on hippocampal neurogenesis: links to cognition and depression. *Neurosci. Biobehav Rev.* **37**, 1346–1362 (2013).
45. Warma, S., Lee, Y., Brietzke, E. & McIntyre, R. S. Microbiome abnormalities as a possible link between diabetes mellitus and mood disorders: pathophysiology and implications for treatment. *Neurosci. Biobehav Rev.* **137**, 104640 (2022).
46. Khawagi, W. Y. et al. Depression and type 2 diabetes: a causal relationship and mechanistic pathway. *Diabetes Obes. Metab.* **26**, 3031–3044 (2024).
47. Li, S. et al. Neurological and metabolic related pathophysiologies and treatment of comorbid diabetes with depression. *CNS Neurosci. Ther.* **30**, e14497 (2024).
48. Uhler, J. P. et al. The UbL protein UBTD1 stably interacts with the UBE2D family of E2 ubiquitin conjugating enzymes. *Biochem. Biophys. Res. Commun.* **443**, 7–12 (2014).
49. Liu, S. et al. Cloning and identification of a novel human ubiquitin-like protein, DC-UbP, from dendritic cells. *Biochem. Biophys. Res. Commun.* **300**, 800–805 (2003).
50. Zhao, L. et al. The ubiquitin-like protein UBTD1 promotes colorectal cancer progression by stabilizing c-Myc to upregulate Glycolysis. *Cell. Death Dis.* **15**, 502 (2024).
51. Zhang, X-W. et al. UBTD1 induces cellular senescence through an UBTD1-Mdm2/p53 positive feedback loop. *J. Pathol.* **235**, 656–667 (2015).
52. Yang, N. et al. CXCR4 mediates matrix stiffness-induced downregulation of UBTD1 driving hepatocellular carcinoma progression via YAP signaling pathway. *Theranostics* **10**, 5790–5801 (2020).
53. Torrino, S. et al. UBTD1 is a mechano-regulator controlling cancer aggressiveness. *EMBO Rep.* **20**, e46570 (2019).
54. Zhao, Z. et al. UBTD1 is a potential prognostic biomarker in colorectal cancer. *Sci. Rep.* **14**, 17926 (2024).
55. Han, D. J. et al. Disruption of adipocyte YAP improves glucose homeostasis in mice and decreases adipose tissue fibrosis. *Mol. Metab.* **66**, 101594 (2022).
56. Claude-Taupin, A., Terzi, F., Codogno, P. & Dupont, N. Yapping at the autophagy door? The answer is flowing in the kidney proximal tubule. *Autophagy* **20**, 1465–1466 (2024).
57. Ruan, S. et al. Knockout of C1q/tumor necrosis factor-related protein-9 aggravates cardiac fibrosis in diabetic mice by regulating YAP-mediated autophagy. *Front. Pharmacol.* **15**, 1407883 (2024).
58. Yang, C. et al. Efficacy and mechanism of Shenqi compound in inhibiting diabetic vascular calcification. *Mol. Med. Camb. Mass.* **29**, 168 (2023).
59. Lv, S. et al. Antidepressant Pharmacological mechanisms: focusing on the regulation of autophagy. *Front. Pharmacol.* **14**, 1287234 (2023).
60. Kamrani, F. et al. Oxidative balance and mental health: exploring the link between prooxidant-antioxidant balance and depression in hypertensive and normotensive individuals, accounting for sex differences. *J. Affect. Disord.* **367**, 391–398 (2024).
61. Feng, Y. et al. Electroacupuncture remodels the extracellular matrix and promotes synaptic plasticity in a mouse model of depression. *Biochem. Biophys. Res. Commun.* **626**, 44–50 (2022).
62. Yu, Z. et al. Decreased density of perineuronal net in prelimbic cortex is linked to Depressive-Like behavior in Young-Aged rats. *Front. Mol. Neurosci.* **13**, 4 (2020).
63. Kennedy-Wood, K., Ng, C. A. S., Alaiyed, S., Foley, P. L. & Conant, K. Increased MMP-9 levels with strain-dependent stress resilience and tunnel handling in mice. *Behav. Brain Res.* **408**, 113288 (2021).
64. Sforzini, L. et al. Transcriptomic profiles in major depressive disorder: the role of immunometabolic and cell-cycle-related pathways in depression with different levels of inflammation. *Mol. Psychiatry* https://doi.org/10.1038/s41380-024-02736-w (2024).

65. Helmy, S. A., Nour, O. A. & Abd El Salam, G. Ameliorative effect of Metformin / alpha-lipoic acid combination on diabetic nephropathy via modulation of YAP/ miR-29a/PTEN/p-AKT axis. *Int. Immunopharmacol.* **135**, 112294 (2024).
66. Zheng, A., Chen, Q. & Zhang, L. The Hippo-YAP pathway in various cardiovascular diseases: focusing on the inflammatory response. *Front. Immunol.* **13**, 971416 (2022).
67. Yao, S. et al. Astrocytic lactate dehydrogenase A regulates neuronal excitability and depressive-like behaviors through lactate homeostasis in mice. *Nat. Commun.* **14**, 729 (2023).
68. Zhang, S. et al. Cognitive dysfunction in diabetes: abnormal glucose metabolic regulation in the brain. *Front. Endocrinol.* **14**, 1192602 (2023).
69. Islam, Z., Nagampalli, R. S. K., Fatima, M. T. & Ashraf, G. M. New paradigm in Ankyrin repeats: beyond protein-protein interaction module. *Int. J. Biol. Macromol.* **109**, 1164–1173 (2018).
70. Sedgwick, S. G. & Smerdon, S. J. The Ankyrin repeat: a diversity of interactions on a common structural framework. *Trends Biochem. Sci.* **24**, 311–316 (1999).
71. Mosavi, L. K., Minor, D. L. & Peng, Z-Y. Consensus-derived structural determinants of the Ankyrin repeat motif. *Proc. Natl. Acad. Sci. U S A*. **99**, 16029–16034 (2002).
72. Wang, X. et al. Regulation of ANKRD9 expression by lipid metabolic perturbations. *BMB Rep.* **42**, 568–573 (2009).
73. Malinouski, M. et al. Genome-wide RNAi ionomics screen reveals new genes and regulation of human trace element metabolism. *Nat. Commun.* **5**, 3301 (2014).
74. Lee, Y. et al. ANKRD9 is associated with tumor suppression as a substrate receptor subunit of ubiquitin ligase. *Biochim. Biophys. Acta Mol. Basis Dis.* **1864**, 3145–3153 (2018).
75. Song, Y. et al. Saikosaponin antidepressant mechanism: improving the sphingolipid metabolism in the cortex via Apolipoprotein E and triggering neurovascular coupling. *Phytomed. Int. J. Phytother. Phytopharm.* **132**, 155829 (2024).
76. Jansen, R. et al. The metabolome-wide signature of major depressive disorder. *Mol. Psychiatry*. https://doi.org/10.1038/s41380-024-02613-6 (2024).
77. Uehara, K., Santoleri, D., Whitlock, A. E. G. & Titchenell, P. M. Insulin regulation of hepatic lipid homeostasis. *Compr. Physiol.* **13**, 4785–4809 (2023).
78. Ağagündüz, D. et al. The roles of dietary lipids and lipidomics in gut-brain axis in type 2 diabetes mellitus. *J. Transl Med.* **21**, 240 (2023).
79. Lee, J., Peña, M. M. O., Nose, Y. & Thiele, D. J. Biochemical characterization of the human copper transporter Ctr1. *J. Biol. Chem.* **277**, 4380–4387 (2002).
80. Liu, X. et al. Correlations among mRNA expression levels of ATP7A, serum ceruloplasmin levels, and neuronal metabolism in unmedicated major depressive disorder. *Int. J. Neuropsychopharmacol.* **23**, 642–652 (2020).
81. Liu, X. et al. Effects of high levels of copper on the Depression-Related memory disorders. *J. Gerontol. Biol. Sci. Med. Sci.* **78**, 611–618 (2023).
82. Tanaka, A. et al. Role of copper ion in the pathogenesis of type 2 diabetes. *Endocr. J.* **56**, 699–706 (2009).
83. Tarnacka, B., Jopowicz, A. & Maślińska, M. Copper, iron, and manganese toxicity in neuropsychiatric conditions. *Int. J. Mol. Sci.* **22**, 7820 (2021).
84. Gembillo, G. et al. Potential role of copper in diabetes and diabetic kidney disease. *Metabolites* **13**, 17 (2022).
85. Liu, R. & Jin, J-P. Calponin isoforms CNN1, CNN2 and CNN3: regulators for actin cytoskeleton functions in smooth muscle and non-muscle cells. *Gene* **585**, 143–153 (2016).
86. Hossain, M. M., Crish, J. F., Eckert, R. L., Lin, J. J. C. & Jin, J-P. h2-Calponin is regulated by mechanical tension and modifies the function of actin cytoskeleton. *J. Biol. Chem.* **280**, 42442–42453 (2005).
87. Logue, M. W. et al. Targeted sequencing of alzheimer disease genes in African Americans implicates novel risk variants. *Front. Neurosci.* **12**, 592 (2018).
88. Chen, M. J. et al. Extracellular signal-regulated kinase regulates microglial immune responses in Alzheimer's disease. *J. Neurosci. Res.* **99**, 1704–1721 (2021).
89. Liu, R. & Jin, J-P. Deletion of Calponin 2 in macrophages alters cytoskeleton-based functions and attenuates the development of atherosclerosis. *J. Mol. Cell. Cardiol.* **99**, 87–99 (2016).
90. Huang, Q-Q. et al. Role of H2-calponin in regulating macrophage motility and phagocytosis. *J. Biol. Chem.* **283**, 25887–25899 (2008).
91. Eapen, V. V., Swarup, S., Hoyer, M. J., Paulo, J. A. & Harper, J. W. Quantitative proteomics reveals the selectivity of ubiquitin-binding autophagy receptors in the turnover of damaged lysosomes by lysophagy. *eLife* **10**, e72328 (2021).
92. Kravić, B. et al. Ubiquitin profiling of lysophagy identifies actin stabilizer CNN2 as a target of VCP/p97 and uncovers a link to HSPB1. *Mol. Cell.* **82**, 2633–2649e7 (2022).
93. Shao, Y. et al. (-)-Epigallocatechin 3-gallate protects pancreatic β-cell against excessive autophagy-induced injury through promoting FTO degradation. *Autophagy* **2024**, 1–18 (2024).
94. Moazzem Hossain, M., Wang, X., Bergan, R. C. & Jin, J-P. Diminished expression of h2-calponin in prostate cancer cells promotes cell proliferation, migration and the dependence of cell adhesion on substrate stiffness. *FEBS Open. Bio.* **4**, 627–636 (2014).
95. Hossain, M. M., Hwang, D-Y., Huang, Q-Q., Sasaki, Y. & Jin, J-P. Developmentally regulated expression of Calponin isoforms and the effect of h2-calponin on cell proliferation. *Am. J. Physiol. Cell. Physiol.* **284**, C156–167 (2003).
96. Yuan, A. & Nixon, R. A. Posttranscriptional regulation of neurofilament proteins and Tau in health and disease. *Brain Res. Bull.* **192**, 115–127 (2023).
97. Cairns, N. J., Lee, V. M. Y. & Trojanowski, J. Q. The cytoskeleton in neurodegenerative diseases. *J. Pathol.* **204**, 438–449 (2004).
98. Wong, G. T. H., Chang, R. C. C. & Law, A. C. K. A breach in the scaffold: the possible role of cytoskeleton dysfunction in the pathogenesis of major depression. *Ageing Res. Rev.* **12**, 67–75 (2013).
99. Gertz, K. et al. The cytoskeleton in couch potato-ism: insights from a murine model of impaired actin dynamics. *Exp. Neurol.* **306**, 34–44 (2018).
100. Wear, M. A. & Cooper, J. A. Capping protein: new insights into mechanism and regulation. *Trends Biochem. Sci.* **29**, 418–428 (2004).
101. Hart, M. C., Korshunova, Y. O. & Cooper, J. A. Vertebrates have conserved capping protein alpha isoforms with specific expression patterns. *Cell. Motil. Cytoskeleton*. **38**, 120–132 (1997).
102. Ohishi, T. et al. Tankyrase-Binding protein TNKS1BP1 regulates actin cytoskeleton rearrangement and Cancer cell invasion. *Cancer Res.* **77**, 2328–2338 (2017).
103. Qiu, J. et al. Gene expression profiles of adipose tissue of high-fat diet-induced obese rats by cDNA microarrays. *Mol. Biol. Rep.* **37**, 3691–3695 (2010).
104. Cingolani, L. A. & Goda, Y. Actin in action: the interplay between the actin cytoskeleton and synaptic efficacy. *Nat. Rev. Neurosci.* **9**, 344–356 (2008).
105. Carlisle, H. J. & Kennedy, M. B. Spine architecture and synaptic plasticity. *Trends Neurosci.* **28**, 182–187 (2005).
106. Ru, Q. et al. TIAM1-mediated synaptic plasticity underlies comorbid depression-like and ketamine antidepressant-like actions in chronic pain. *J. Clin. Invest.* **132**, e158545 (2022).
107. Fan, Y., Tang, X., Vitriol, E., Chen, G. & Zheng, J. Q. Actin capping protein is required for dendritic spine development and synapse formation. *J. Neurosci. Off J. Soc. Neurosci.* **31**, 10228–10233 (2011).
108. Simonetti, B. & Cullen, P. J. Actin-dependent endosomal receptor recycling. *Curr. Opin. Cell. Biol.* **56**, 22–33 (2019).

109. Wang, D. et al. Capping protein regulates endosomal trafficking by controlling F-actin density around endocytic vesicles and recruiting RAB5 effectors. *eLife* **10**, e65910 (2021).
110. Mendoza, P., Díaz, J., Silva, P. & Torres, V. A. Rab5 activation as a tumor cell migration switch. *Small GTPases*. **5**, e28195 (2014).
111. Parachoniak, C. A. & Park, M. Dynamics of receptor trafficking in tumorigenicity. *Trends Cell. Biol.* **22**, 231–240 (2012).
112. Fletcher, S. J. & Rappoport, J. Z. Moving forward: polarised trafficking in cell migration. *Trends Cell. Biol.* **20**, 71–78 (2010).
113. Hers, I., Vincent, E. E. & Tavaré, J. M. Akt signalling in health and disease. *Cell. Signal.* **23**, 1515–1527 (2011).
114. Nicholson, K. M. & Anderson, N. G. The protein kinase B/Akt signalling pathway in human malignancy. *Cell. Signal.* **14**, 381–395 (2002).
115. Ji, Y. et al. Xiaoyao pills ameliorate Depression-like behaviors and oxidative stress induced by olfactory bulbectomy in rats via the activation of the PIK3CA-AKT1-NFE2L2/BDNF signaling pathway. *Front. Pharmacol.* **12**, 643456 (2021).
116. Manning, B. D. & Cantley, L. C. AKT/PKB signaling: navigating downstream. *Cell* **129**, 1261–1274 (2007).
117. Huang, X., Liu, G., Guo, J. & Su, Z. The PI3K/AKT pathway in obesity and type 2 diabetes. *Int. J. Biol. Sci.* **14**, 1483–1496 (2018).
118. Whiteman, E. L., Cho, H. & Birnbaum, M. J. Role of Akt/protein kinase B in metabolism. *Trends Endocrinol. Metab. TEM*. **13**, 444–451 (2002).
119. Zhang, J. et al. Polysaccharides from Cynanchum auriculatum royle ex Wight ameliorate symptoms of hyperglycemia by regulating gut microbiota in type 2 diabetes mellitus mice. *Int. J. Biol. Macromol.* **299**, 139878 (2025).
120. Liu, L. et al. The effect of Banxia-houpo Decoction on CUMS-induced depression by promoting M2 microglia polarization via TrkA/Akt signalling. *J. Cell. Mol. Med.* **27**, 3339–3353 (2023).
121. Chandran, A. et al. Reduced phosphorylation of the mTOR signaling pathway components in the amygdala of rats exposed to chronic stress. *Prog Neuropsychopharmacol. Biol. Psychiatry*. **40**, 240–245 (2013).
122. Machado-Vieira, R. et al. Decreased AKT1/mTOR pathway mRNA expression in short-term bipolar disorder. *Eur. Neuropsychopharmacol. J. Eur. Coll. Neuropsychopharmacol.* **25**, 468–473 (2015).
123. Zang, X. et al. Electroconvulsive therapy combined with Esketamine improved depression through PI3K/AKT/GLT-1 pathway. *J. Affect. Disord*. **368**, 282–294 (2025).
124. Li, N. et al. mTOR-dependent synapse formation underlies the rapid antidepressant effects of NMDA antagonists. *Science* **329**, 959–964 (2010).
125. Zhang, Z. et al. Bavachin ameliorates neuroinflammation and depressive-like behaviors in streptozotocin-induced diabetic mice through the Inhibition of PKCδ. *Free Radic Biol. Med.* **213**, 52–64 (2024).
126. Ismail, T. R., Yap, C. G., Naidu, R., Shri, L. & Pamidi, N. Environmental enrichment and the combined interventions of EE and Metformin enhance hippocampal neuron survival and hippocampal-dependent memory in type 2 diabetic rats under stress through the BDNF-TrkB signaling pathways. *Biomed. Pharmacother. Biomed. Pharmacother.* **175**, 116729 (2024).
127. Dutheil, S., Ota, K. T., Wohleb, E. S., Rasmussen, K. & Duman, R. S. High-Fat diet induced anxiety and anhedonia: impact on brain homeostasis and inflammation. *Neuropsychopharmacol. Off Publ Am. Coll. Neuropsychopharmacol.* **41**, 1874–1887 (2016).
128. Tang, Y. et al. The effect and mechanism of Jiao-tai-wan in the treatment of diabetes mellitus with depression based on network Pharmacology and experimental analysis. *Mol. Med. Camb. Mass.* **27**, 154 (2021).
129. Onisiforou, A. & Zanos, P. One path, two solutions: Network-based analysis identifies targetable pathways for the treatment of comorbid type II diabetes and neuropsychiatric disorders. *Comput. Struct. Biotechnol. J.* **23**, 3610–3624 (2024).
130. Shen, J-D., Wei, Y., Li, Y-J., Qiao, J-Y. & Li, Y-C. Curcumin reverses the depressive-like behavior and insulin resistance induced by chronic mild stress. *Metab. Brain Dis.* **32**, 1163–1172 (2017).
131. Banks, W. A., Owen, J. B. & Erickson, M. A. Insulin in the brain: there and back again. *Pharmacol. Ther.* **136**, 82–93 (2012).
132. Qiu, W. et al. Xiaoyaosan ameliorates depressive-like behavior and susceptibility to glucose intolerance in rat: involvement of LepR-STAT3/PI3K pathway in hypothalamic arcuate nucleus. *BMC Complement. Med. Ther.* **23**, 116 (2023).
133. Li, J. et al. PI3K/AKT/JNK/p38 signalling pathway-mediated neural apoptosis in the prefrontal cortex of mice is involved in the antidepressant-like effect of Pioglitazone. *Clin. Exp. Pharmacol. Physiol.* **45**, 525–535 (2018).
134. Su, P. et al. Modified Xiaoyao San reverses lipopolysaccharide-induced depression-like behavior through suppressing microglia M1 polarization via enhancing autophagy involved in PI3K/Akt/mTOR pathway in mice. *J. Ethnopharmacol.* **315**, 116659 (2023).
135. Li, X. et al. AKT and MAPK signaling pathways in hippocampus reveals the pathogenesis of depression in four stress-induced models. *Transl. Psychiatry*. **13**, 200 (2023).
136. Brivio, P. et al. Chronic restraint stress inhibits the response to a second hit in adult male rats: A role for BDNF signaling. *Int. J. Mol. Sci.* **21**, 6261 (2020).
137. Cross, D. A., Alessi, D. R., Cohen, P., Andjelkovich, M. & Hemmings, B. A. Inhibition of glycogen synthase kinase-3 by insulin mediated by protein kinase B. *Nature* **378**, 785–789 (1995).
138. Grimes, C. A. & Jope, R. S. The multifaceted roles of glycogen synthase kinase 3beta in cellular signaling. *Prog Neurobiol.* **65**, 391–426 (2001).
139. Laplante, M. & Sabatini, D. M. mTOR signaling in growth control and disease. *Cell* **149**, 274–293 (2012).
140. Sarkar, S. Regulation of autophagy by mTOR-dependent and mTOR-independent pathways: autophagy dysfunction in neurodegenerative diseases and therapeutic application of autophagy enhancers. *Biochem. Soc. Trans.* **41**, 1103–1130 (2013).
141. Livak, K. J. & Schmittgen, T. D. Analysis of relative gene expression data using Real-Time quantitative PCR and the 2 – ΔΔCT method. *Methods* **25**, 402–408 (2001).
142. Zhao, M. et al. A machine learning-based diagnosis modelling of type 2 diabetes mellitus with environmental metal exposure. *Comput. Methods Programs Biomed.* **235**, 107537 (2023).
143. Nock, M. K. et al. Cross-national analysis of the associations among mental disorders and suicidal behavior: findings from the WHO world mental health surveys. *PLoS Med.* **6**, e1000123 (2009).
144. de Beurs, D., Ten Have, M., Cuijpers, P. & de Graaf, R. The longitudinal association between lifetime mental disorders and first onset or recurrent suicide ideation. *BMC Psychiatry*. **19**, 345 (2019).
145. Purselle, D. C. & Nemeroff, C. B. Serotonin transporter: a potential substrate in the biology of suicide. *Neuropsychopharmacol. Off Publ Am. Coll. Neuropsychopharmacol.* **28**, 613–619 (2003).
146. Miller, J. M. et al. Positron emission tomography quantification of serotonin transporter in suicide attempters with major depressive disorder. *Biol. Psychiatry*. **74**, 287–295 (2013).
147. Ding, R. et al. Trajectories and predictors of suicidal ideation in clinical characteristics and Pharmacological treatments for major depressive disorder: a study based on a National multi-centered prospective cohort. *Transl. Psychiatry*. **14**, 422 (2024).
148. Wang, Q. et al. Connectomics-based resting-state functional network alterations predict suicidality in major depressive disorder. *Transl. Psychiatry*. **13**, 365 (2023).

Author contributions

Y.Z. and L.W.: writing—original draft preparation, writing—review and editing, performed experiments, visualization; C.Z. and H.X.: writing—original draft preparation, data curation, formal analysis, Conceptualization; Z.C. and W.L.: data curation, formal analysis; L.C. and Y.Q.: funding acquisition, Conceptualization, methodology, writing—review and editing. All co-authors have read and approved the final version of the manuscript.

Funding
This study was supported by Zhejiang Provincial Natural Science Foundation of China under Grant No. LQ24H270013, Zhejiang Province Traditional Chinese Medicine Science and Technology Plan Key Project No. 2022ZZ010 and Project No.2024ZR102.

Competing interests
The authors declare no competing interests.

Ethics approval and consent to participate
The animal study protocol was approved by the Institutional Review Board of Animal Experiments of Zhejiang Chinese Medical University for studies involving animals. All procedures were conducted in full compliance with the ARRIVE guidelines 2.0.

Additional information
Supplementary Information The online version contains supplementary material available at https://doi.org/10.1038/s41598-025-01175-z.

Correspondence and requests for materials should be addressed to L.C. or Y.Q.